

AD A063485

LEVEL

12

SYSTEMS, SCIENCE AND SOFTWARE

SSS-R-78-3690

SOURCE AMPLITUDES OF NTS EXPLOSIONS INFERRED FROM
RAYLEIGH WAVES AT ALBUQUERQUE AND TUCSON

T. C. BACHE
W. L. RODI
B. F. MASON

TOPICAL REPORT

DDC
RECEIVED
JAN 17 1979
REF ID: A6471
C

SPONSORED BY
ADVANCED RESEARCH PROJECTS AGENCY
ARPA ORDER No. 2551

This research was supported by the Advanced Research Projects Agency of the Department of Defense and was monitored by AFTAC/VSC, Patrick Air Force Base, Florida, 32925, under Contract No. F08606-76-C-0041.

The views and conclusions contained in this document are those of the authors and should not be interpreted as necessarily representing the official policies, either expressed or implied, of the Advanced Research Projects Agency, the Air Force Technical Applications Center, or the U. S. Government.

APPROVED FOR PUBLIC RELEASE, DISTRIBUTION UNLIMITED

JUNE 1978

P. O. BOX 1620, LA JOLLA, CALIFORNIA 92038, TELEPHONE (714) 453-0060

57

AFTAC Project Authorization No. VELA/T/7712/B/ETR

ARPA Order 2551, Program Code 8F10

Effective Date of Contract: October 1, 1976

Contract Expiration Date: September 30, 1978

Amount of Contract: \$435,087

Contract No. F08606-76-C-0041

Principal Investigator and Phone No.

Dr. Thomas C. Bache, (714) 453-0060, Ext. 337

Project Scientist and Phone No.

Captain Michael J. Shore, (202) 325-7581

UNCLASSIFIED

SECURITY CLASSIFICATION OF THIS PAGE (When Data Entered)

REPORT DOCUMENTATION PAGE		READ INSTRUCTIONS BEFORE COMPLETING FORM
1. REPORT NUMBER	2. GOVT ACCESSION NO.	3. RECIPIENT'S CATALOG NUMBER
4. TITLE (and Subtitle)		5. TYPE OF REPORT & PERIOD COVERED
6. SOURCE AMPLITUDES OF NTS EXPLOSIONS INFERRED FROM RAYLEIGH WAVES AT ALBUQUERQUE AND TUCSON		7. PERFORMING ORG. REPORT NUMBER 8. CONTRACT OR GRANT NUMBER(S)
7. AUTHOR(s)		9. PERFORMING ORGANIZATION NAME AND ADDRESS Systems, Science and Software P. O. Box 1620 La Jolla, California 92038
10. PROGRAM ELEMENT, PROJECT, TASK AREA & WORK UNIT NUMBERS		11. CONTROLLING OFFICE NAME AND ADDRESS VELA Seismological Center 312 Montgomery Street Alexandria, Virginia 22314
12. MONITORING AGENCY NAME & ADDRESS (if different from Controlling Office)		13. REPORT DATE 14. NUMBER OF PAGES 91
15. SECURITY CLASS. (of this report)		16. DISTRIBUTION STATEMENT (of this Report)
17. DISTRIBUTION STATEMENT (of the document entered in Block 20, if different from Report)		18. DECLASSIFICATION DOWNGRADING SCHEDULE
19. KEY WORDS (Continue on reverse side if necessary and identify by block number) Nuclear Explosion Seismology Rayleigh Waves Surface Wave Magnitude Synthetic Seismograms		
20. ABSTRACT (Continue on reverse side if necessary and identify by block number) Comparing observed and synthetic seismograms, source amplitudes of NTS explosions are inferred from Rayleigh wave recordings from the WSSN stations at Albuquerque, New Mexico (ALQ) and Tucson, Arizona (TUC). The potential influence of source complexities, particularly surface spallation and related phenomena, is studied in detail.		
		(cont'd)

UNCLASSIFIED

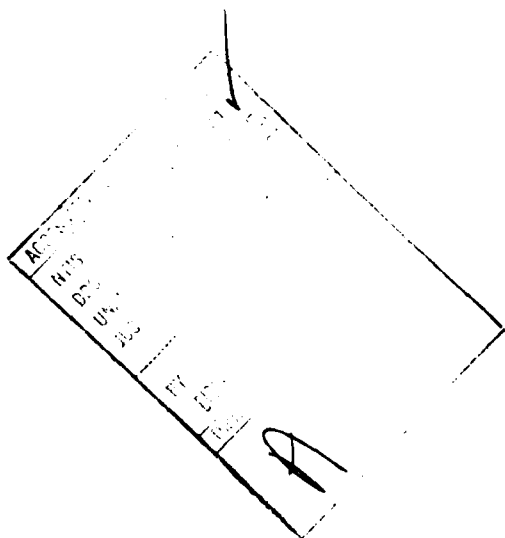
SECURITY CLASSIFICATION OF THIS PAGE(When Data Entered)

20. ABSTRACT (continued)

As described in earlier work by Bache, Rodi and Harkrider, the earth model for the synthetic were converted from observations at ALQ and TUC. The agreement of observed and synthetic seismograms is quite good and is sensitive to important features of the source.

The events studied are in three distinct areas, Yucca Flat, Pahute Mesa and PILEDRIVER in climax granite. All events were below the water table and the yields varied from 40 to 200 KT. Within each group the mean static value of the reduced displacement potential (Ψ_∞) was determined at a fixed scaled yield, assuming a spherically symmetric point source. The source is then modified to study the effect of: (1) the addition of a double-couple component; (2) the addition of a surface impulse associated with impact of the material spalled from the surface; (3) loss of energy from the free surface reflected waves due to spallation. Comparing observed and synthetic seismograms, the extent of the effect of these secondary phenomena is outlined.

For Yucca Flat and Pahute Mesa events the inferred source amplitudes are in general agreement with values obtained by other methods. The spall impulse is too small to be of much importance. More likely to be important, especially for the Pahute Mesa events, is the loss of energy from the upgoing waves. For PILEDRIVER the double-couple and attenuation of upgoing waves dominate the source determination. Correcting for these phenomena, the explosion source level (Ψ_∞) is considerably smaller than has usually been supposed.



UNCLASSIFIED

SECURITY CLASSIFICATION OF THIS PAGE(When Data Entered)

TABLE OF CONTENTS

<u>Section</u>		<u>Page</u>
I.	INTRODUCTION AND SUMMARY	1
	1.1 Introduction	1
	1.2 Outline of the Analysis	3
	1.3 Summary of Results	6
	1.4 Conclusions	8
II.	COMPARISON OF THEORETICAL AND OBSERVED RAYLEIGH WAVEFORMS	9
III.	PARAMETRIC DEPENDENCE OF RAYLEIGH WAVE AMPLITUDES	17
IV.	SOURCE ESTIMATES ASSUMING SPHERICAL SYMMETRY	26
V.	CORRECTION FOR THE EFFECTS OF A DOUBLE-COUPLE ENHANCEMENT OF THE SOURCE	49
VI.	CORRECTION FOR THE EFFECT OF SURFACE SPALLATION	55
	6.1 Introduction	55
	6.2 Estimation of the Impulse due to Spall Closure	56
	6.3 Calculation of Rayleigh Waves from the Spall Closure Impulse	59
	6.4 Modification of the Explosion Source to Account for Energy Lost to Spallation	64
	6.5 Simultaneous Correction for the Spall Impulse and Double-Couple Contributions to the Source	74
VII.	EXAMINATION OF THE DIFFERENCES BETWEEN THE ALQ AND TUC SOURCE ESTIMATES	79
VIII.	CONCLUSIONS	84
	ACKNOWLEDGMENT	88
	REFERENCES	89

LIST OF ILLUSTRATIONS

<u>Figure</u>		
1. Typical seismograms are shown for six events recorded at each station. The first three events in each column are plotted from hand-digitized data while the others are tracings from the film records.	10	
2. The observed phase and group velocities are shown for three events at NTS to ALQ and TUC.	12	
3. The inversion model for the NTS-ALQ path is shown together with a comparison of its predicted dispersion with the observed NTS-ALQ dispersion	13	
4. The inversion model for the NTS-TUC path is shown together with a comparison of its predicted dispersion with the observed NTS-TUC dispersion	14	
5. Theoretical and observed seismograms are compared at ALQ and TUC for events in three test areas at NTS	15	
6. The density, shear and compressional wave velocities are plotted versus depth for the three test areas at NTS.	19	
7. The source amplification factor is shown at left for the three source areas studied. At right is the transmission coefficient $T(\omega)$ for the six source-path combinations	20	
8. The Q_8 models used to derive $\gamma(\omega)$ are shown at left for the NTS-ALQ and NTS-TUC paths with d denoting layer thickness.	23	
9. The amplitude of the source function for the theoretical seismograms is plotted with the frequency axis scaled to 100 KT and the amplitude axis to 0.02 KT.	27	
10. Airy phase amplitudes for Yucca Flat explosions recorded at ALQ and TUC are plotted versus explosion yield	28	

LIST OF ILLUSTRATIONS (continued)

<u>Figure</u>		<u>Page</u>
11.	Airy phase amplitudes for Pahute Mesa explosions recorded at ALQ and TUC are plotted versus explosion yield	29
12.	Seismograms are shown at three ranges for two test areas	32
13.	The Ψ_∞ values (at 0.02 KT) are plotted versus explosion yield for the Yucca Flat and Pahute Mesa events.	35
14.	Source spectra scaled to 0.02 KT are shown for the indicated materials.	40
15.	Source spectra scaled to 0.02 KT are shown for calculations 131 ($\phi_0 = 4.4$ percent), 132 ($\phi_0 = 3.0$ percent) and 133 ($\phi_0 = 1.6$ percent) for Yucca Flat wet tuff.	41
16.	Source spectra scaled to 0.02 KT are shown for calculations 124 ($P_C = 0.5$) and 125 ($P_C = 1.0$) in Pahute Mesa rhyolite	42
17.	The analytical source functions calculated by Haskell (1967) from data given by Werth and Herbst (1963) are shown with the amplitudes scaled to 0.02 KT and the frequency axis scaled to 5 KT	43
18.	The source function amplitudes computed from PILEDRIVER observed velocity records at two ranges are compared to the theoretical source 130.	44
19.	Theoretical seismograms for PILEDRIVER at TUC are shown for a composite source including the explosion plus a strike-slip double-couple .	53
20.	The effect of the spall closure impulse on the Rayleigh waves for Yucca Flat explosions is shown for two lag times and two spall impulse amplitudes	62
21.	Synthetic seismograms for a variety of source representations for a Yucca Flat event . . .	68

LIST OF ILLUSTRATIONS (continued)

<u>Figure</u>		<u>Page</u>
22.	Synthetic seismograms for a variety of source representations for PILEDRIVER. . . .	71
23.	Synthetic seismograms for a variety of source representations for a Pahute Mesa event. . . .	73
24.	Theoretical seismograms at TUC for PILEDRIVER represented by a source including explosion and double-couple components	75
25.	The observation of the Yucca Flat event TAN at TUC is compared to synthetic seismograms computed with two attenuation models	83

LIST OF TABLES

<u>Table</u>		<u>Page</u>
1.	Description of Selected Events	11
2.	Values of the Excitation Factor $\mu_s K_{s1}$ A_{R1}/c_1	21
3.	Attenuation Parameters, $\gamma(\omega)$, for the Theoretical Seismograms of Figure 5	24
4.	Inferred Values of Ψ_∞ Scaled to 0.02 KT . .	36
5.	Linear Regression Fit to the Inferred Ψ_∞ Data	37
6.	Comparison of Theoretical and Observed Ψ_∞ Values to those Inferred from the ALQ and TUC Rayleigh Waves. All Ψ_∞ Values are Scaled to 0.02 KT	47
7.	Correction of the Rayleigh Wave Amplitudes for the Double-Couple Solution of Toksöz and Kehrer (1972)	50
8.	Inferred Ψ_∞ Values Corrected by the Double-Couple Factors from Table 7	54
9.	Impulse for a Fixed Ratio of Spall Closure to Explosion Rayleigh Waves.	65
10.	Simultaneous Correction for the Effect of Spallation and a Superimposed Double-Couple	76

I. INTRODUCTION AND SUMMARY

1.1 Introduction

Commonly used methods for estimating the yield of foreign underground nuclear explosions rely on the use of empirical relations between body (m_b) and surface (M_s) wave magnitudes and yield. The difficulty with empirical relationships is that they can be systematically in error when applied to events outside the empirical data base. This problem is widely recognized and, as a result, there is considerable interest in developing a clear understanding of the important parameters that control the seismic signatures of underground explosions.

In this report we describe a study of NTS explosions in which we have attempted to model in great detail the recorded Rayleigh waves at two WWSSN stations: Albuquerque, New Mexico (ALQ) and Tucson, Arizona (TUC). We find that our synthetic waveforms are in excellent agreement with the observations. This suggests that most of the important contributing factors are properly represented by our models.

The main objectives of the work described in this report are to use the comparison of synthetic and observed Rayleigh waves to infer the long period amplitude of the NTS explosion source and to explore the potential influence of supposed source complexities, particularly surface spallation and related phenomena. In pursuing these objectives we address the following questions:

- How accurately can the Rayleigh wave signature of NTS explosions be modeled with plane-layered elastic models for the travel path?
- Is a spherically symmetric point source adequate for modeling the source?

- What is the effect of surface spallation on the Rayleigh wave?
- What is the effect of tectonic strain release on the Rayleigh wave?
- What is the source amplitude and how does it depend on source material, source depth and yield?
- How much scatter is to be expected for events in relatively homogeneous regions (e.g., below the water table at Yucca Flat) and what are the main causes of this scatter?

We have chosen to use data from the stations ALQ and TUC because the data was conveniently available and because these stations are at an excellent range (700 to 950 km) for studying NTS explosions. They are close enough to record many of the smaller yield events, while being at a range where the trace is dominated by the fundamental mode Rayleigh wave. At their normal gain setting the Rayleigh wave trace can be measured for yields as large as 200 to 300 KT.

The first step in our analysis of the ALQ and TUC data was to determine the crustal structure along the two paths and this work was reported by Bache, Rodi and Harkrider (1978). The crustal models were determined by inverting the phase and group velocities inferred directly from the ALQ and TUC recordings of NTS explosions. The inverted crustal structures were satisfying in that they were simple (few major discontinuities were present), agreed with other available data (e.g., from refraction studies) for these paths and gave an excellent fit to the dispersion data. Using attenuation models based on data given by Mitchell (1975), Bache, Rodi and Harkrider (1978) computed synthetic seismograms for representative events in several test areas at NTS and found that the agreement of theoretical and observed waveforms was very good.

1.2 Outline of the Analysis

The results of the earlier work gave reason to believe that we could quite accurately account for the path effects for NTS explosions observed at ALQ and TUC and thus determine the characteristics of the source. This is the primary objective of the work described in this report. In outline form our report includes the following:

- A. The pertinent results of the Bache, Rodi and Harkrider study are summarized (Section II).
- B. The theoretical formulation used to compute synthetic Rayleigh wave seismograms is summarized with particular attention to the parameters that control the amplitude (Section III).
- C. A spherically symmetric source represented by a reduced displacement potential is assumed. Then for each of the test areas studied (Yucca Flat, Pahute Mesa and PILEDRIVER), the Rayleigh wave amplitude is directly proportional to the static value of the reduced displacement potential (Ψ_∞). Comparing theoretical and observed seismograms, a Ψ_∞ is determined from each station for each event and the values are scaled to a common yield. The important results are as follows (Section IV):
 - At ALQ the mean values of the Ψ_∞ scaled to 0.02 KT are 9.1 m^3 for the 17 Yucca Flat events, 6.6 m^3 for the 7 Pahute Mesa events and 3.9 for PILEDRIVER.* Only events below the water table with yields from 40 to 200 KT were studied. The standard deviation for each population is about 40 percent of the mean.
 - The Ψ_∞ inferred from the TUC records are consistently 1.5 times larger than from ALQ.

*Throughout the report we use the notation Ψ_∞ for both the absolute value for a given event and for values scaled by the cube-root of the yield to 0.02 KT. When there is any possibility of confusion about which kind of value is meant, we use the notation Ψ_∞^{02} to indicate the common yield value.

- For similar materials the Rayleigh waves are proportional to $\mu_s \Psi_\infty$, where μ_s is the average shear modulus in the source region. Variations in μ_s and errors in the official yield are two sources of random scatter in the Ψ_∞ in a particular area.
- Random effects can plausibly account for at most half the scatter in the inferred source levels for each population. The remainder of the scatter appears to be due to real differences among the source levels of the different events in each population.
- The slope of the $\log \Psi_\infty$ -log yield curve (comparable to M_s -log yield) cannot be determined with confidence for the rather narrow yield range represented in our data.

D. The Ψ_∞ values from this analysis of Rayleigh waves are compared to estimates of Ψ_∞ made by other methods; for example, from close-in methods, from far-field body and surface waves or from theoretical considerations. Our values are within the range expected from this other work except for PILEDRIVER where our value is low (Section IV).

E. The assumption that the source is spherically symmetric is clearly an oversimplification. Using results obtained by Toksöz and Kehrer (1972), we correct our solution for the effect of a double-couple component in the source. We find that the double-couple has virtually no effect on the waveform, but simply scales the amplitude. If the values given by Toksöz and Kehrer are typical, some 15 to 20 percent of the discrepancy between the ALQ and TUC solutions for the Yucca Flat and Pahute Mesa Ψ_∞ is due to the double-couple. The mean $\Psi_\infty^{.02}$ values at ALQ are reduced from 9.1 and 6.6 to 8.1 and 4.3 for these two areas. For PILEDRIVER Toksöz and Kehrer predict a much larger effect on the Rayleigh waves at these two stations. Their solution actually increases the discrepancy between the values obtained at the two stations, though it is quite sensitive to small errors in the double-couple orientation. Further, the double-couple contribution so dominates the solution that the $\Psi_\infty^{.02}$ required to match the data at ALQ is reduced to about 1.0 (Section V).

F. The impulse delivered by the impact of the large mass of spalled material returning to the free surface has been supposed to have some significant effect on the Rayleigh wave signature of explosions (e.g., Viecelli, 1973). Using estimates for the spall impulse given by Viecelli (1973) and somewhat larger estimates given by Sobel (1978), we compute expected Rayleigh waves at ALQ and TUC to determine its effect. We find it to be quite small. It seems implausible to suppose that the spall impulse could change the Rayleigh wave amplitude by more than 5 to 10 percent (Section VI).

G. A spall-related phenomenon that may be much more significant is the associated loss of energy from the waves traveling upward from the source. We explore the potential effect by simply deleting a portion of the upgoing waves from the solution. A more appropriate filter may be frequency-dependent, having its primary effect on the short periods, but at present we have no results to support this conjecture. The events at Yucca Flat are quite insensitive to the suppression of the upgoing waves. The effect at Pahute Mesa is much larger with suppression of half the upgoing waves leading to a decrease of about 25 percent in the amplitude. PILEDRIVER is extremely sensitive to the amount of upgoing waves suppressed and this is a very important parameter for events in granite. If we suppose that 50 percent of the upgoing wave is lost to spallation or scattering, the Rayleigh wave amplitude is reduced by about 40 percent. Suppression of 25 percent of the upgoing waves caused a decrease of about 20 percent in the amplitude (Section VI).

H. We carefully examine the factors that control the amplitude of the synthetic seismograms to determine why the source level inferred from the TUC observations is about 1.5 times larger than that inferred from the ALQ observations. A partial explanation is provided by the presence of asymmetries at the source, particularly the double-couple (E.), but a substantial amount remains. There are four main features of the theoretical calculation that are examined closely; the dispersion, the model for the source region, the transition between the local source structure and average path structure and the inelastic attenuation (Q) for the two paths. Rather than from any one factor, the differences in the source estimates seem to be

due to contributions from each of these. Errors in the dispersion and attenuation are small, but tend in the right direction. The main source of error is probably associated with the failure of plane-layered laterally homogeneous models to precisely represent the complex real earth. We recommend that the answers from the two stations be averaged, but give more weight to those from ALQ. A better definition of the true source amplitude would probably be achieved by carrying out the same analysis for more stations and averaging the results (Section VII).

1.3 Summary of Results

In our analysis we divided the explosions into three groups (Yucca Flat, Pahute Mesa and PILEDRIVER) separated geographically and by the average material properties at the source. Using plane-layered earth models, synthetic seismograms were computed that give excellent agreement with the observed waveforms. For the source we used four different models that were combined in various ways. These are:

- A spherically symmetric point source given by a reduced displacement potential.
- A reduced displacement potential source with a portion of the upgoing waves suppressed.
- A downward impulse representing the impact of the spalled material.
- A double-couple.

The source quantity most directly related to explosion yield is the static level of the reduced displacement potential (Ψ_∞).^{*} We first estimate this quantity assuming the source is spherically symmetric, then correct these estimates for other effects. Our best estimates for the mean Ψ_∞ scaled to 0.02 KT in each area are as follows:

^{*}The relationship between Ψ_∞ and yield is dependent on the local material properties and is a subject for separate discussion (e.g., Cherry, et al., 1975)

	<u>Yucca Flat</u>	<u>Pahute Mesa</u>	<u>PILEDRIVER</u>
1. Assume spherical symmetry (Table 4)	10.5	8.1	4.7
2. Correct for observed double-couple (Table 8)	8.3	4.8	1.4
3. Correct for spallation* (Figures 21-23)	11.4	10.0	5.9
4. Simultaneously correct for spallation and double-couple (Section 6.5)	9.1	5.8	1.8 2.7 [†]

* The spall impact makes little contribution. The main effect is the suppression of upgoing waves from the source. This estimate is based on suppression of 75 percent of these waves.

† 25 percent of the upgoing waves from both the explosion and double-couple are suppressed. For Yucca Flat and Pahute Mesa, the suppression is only applied to the explosion waves.

Throughout the report values are determined separately for the two stations ALQ and TUC. The "best" estimates given above were determined by averaging the two with the ALQ values given double weight.

The values given represent mean values and individual events can deviate substantially from these. The corrections for the double-couple and spallation contributions are again based on mean values, but these effects must vary widely from event to event. In fact, variation in these effects is likely to be responsible for a large portion of what we have called "real" source level variations; that is, variations that cannot be attributed to random errors in our modeling procedure. The effect of the double-couple can be reduced by averaging values from many azimuths, while the spallation effects are not likely to depend on azimuth.

This report is concerned with mean source amplitudes for selected populations of events. The values for individual events are available for those with the proper security clearance (Bache, 1978). A substantial amount of the deviation of individual events from the mean may be explicable from known peculiarities of these events. We have not attempted to correlate our values with candidate parameters like the velocities or other material properties near the event. This may be a useful exercise for the future.

1.4 Conclusions

Our major conclusions are summarized in Section VIII. Most important is our demonstration that available techniques are capable of modeling surface wave signatures of underground explosions in considerable detail. The amplitude of the source can thus be inferred from a comparison of synthetic and observed seismograms. Applied to foreign explosions, this would lead to yield estimates that are independent of the estimates from empirical M_s -yield curves.

II. COMPARISON OF THEORETICAL AND OBSERVED RAYLEIGH WAVEFORMS

Typical ALQ and TUC recordings of NTS explosions are shown in Figure 1, and the pertinent data for these events are summarized in Table 1 (Springer and Kinnaman, 1971). There is a clearly defined maximum phase on each record. Within the test area groupings (PILEDRIVER, Pahute Mesa, Yucca Flat) the waveforms are remarkably consistent for the more than 50 events examined at each station. This makes it possible to select representative events from each group for closer analysis.

Bache, Rodi and Harkrider (1978) inferred crustal models for the NTS-TUC and NTS-ALQ paths. This was done in the following way:

1. Seismograms for PILEDRIVER, DURYEA and TAN at each station (Figure 1) were hand-digitized.
2. The phase and group velocities were derived from the seismograms. The results are shown in Figure 2.
3. Using linear inversion, crustal structure were inferred from the phase and group velocity data. The crustal structures were also constrained to be consistent with other information about the paths. The structures and the agreement observed and theoretical dispersion are shown in Figures 3 and 4.
4. Using methods outlined in the next section, theoretical seismograms were computed for each station-event pair. The comparison to the observations is shown in Figure 5.

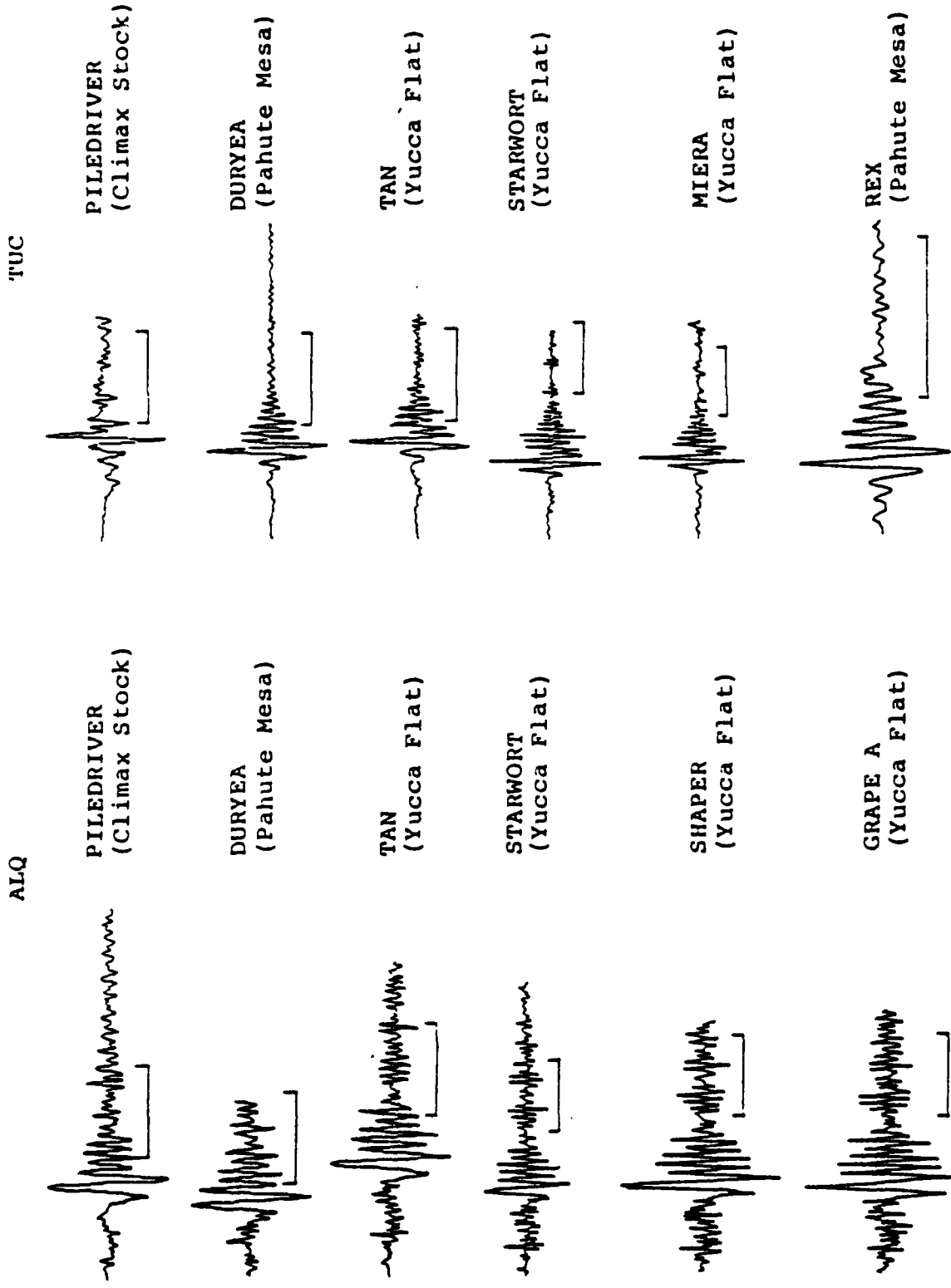


Figure 1. Typical seismograms are shown for six events recorded at each station. The first three events in each column are plotted from hand-digitized data while the others are tracings from the film records. All seismograms are not on the same time scale - one minute is indicated on each record.

TABLE 1
DESCRIPTION OF SELECTED EVENTS

<u>Name and Date</u>	<u>Shot Time (GMT)</u>	<u>Yield (kt)</u>	<u>Depth (km)</u>	<u>Source Area and Material</u>	<u>TUC Azimuth, Distance</u>	<u>ALQ Azimuth, Distance</u>
PILEDRIVER 6/2/66	1530:00:09	~ 56	0.463	Climax Stock Granite	137° 720.1	103° 900.4
TAN 6/3/66	1400:00:04	Low-Intermediate	0.544	Yucca Flat Tuff	136° 714.1	102° 894.7
DURYEA 4/14/66	1413:43:10	65	0.560	Pahute Mesa Rhyolite	135° 752.6	103° 933.2
STARHORN 4/26/73	1715:00:16	65	0.564	Yucca Flat Tuff	136° 719.9	103° 898.0
SHAPER 3/23/70	2305:00:04	Low-Intermediate	0.561	Yucca Flat Tuff	136° 714.7	103° 893.9
MIERA 3/8/73	1610:00:19	Low-Intermediate	0.569	Yucca Flat Tuff	136° 716.4	103° 894.8
GRAPE A 12/17/69	1500:00:04	Low-Intermediate	0.551	Yucca Flat Tuff	136° 713.3	103° 892.1
REX 2/24/66	1555:07:04	16	0.672	Pahute Mesa Tuff	135° 755.0	103° 934.2

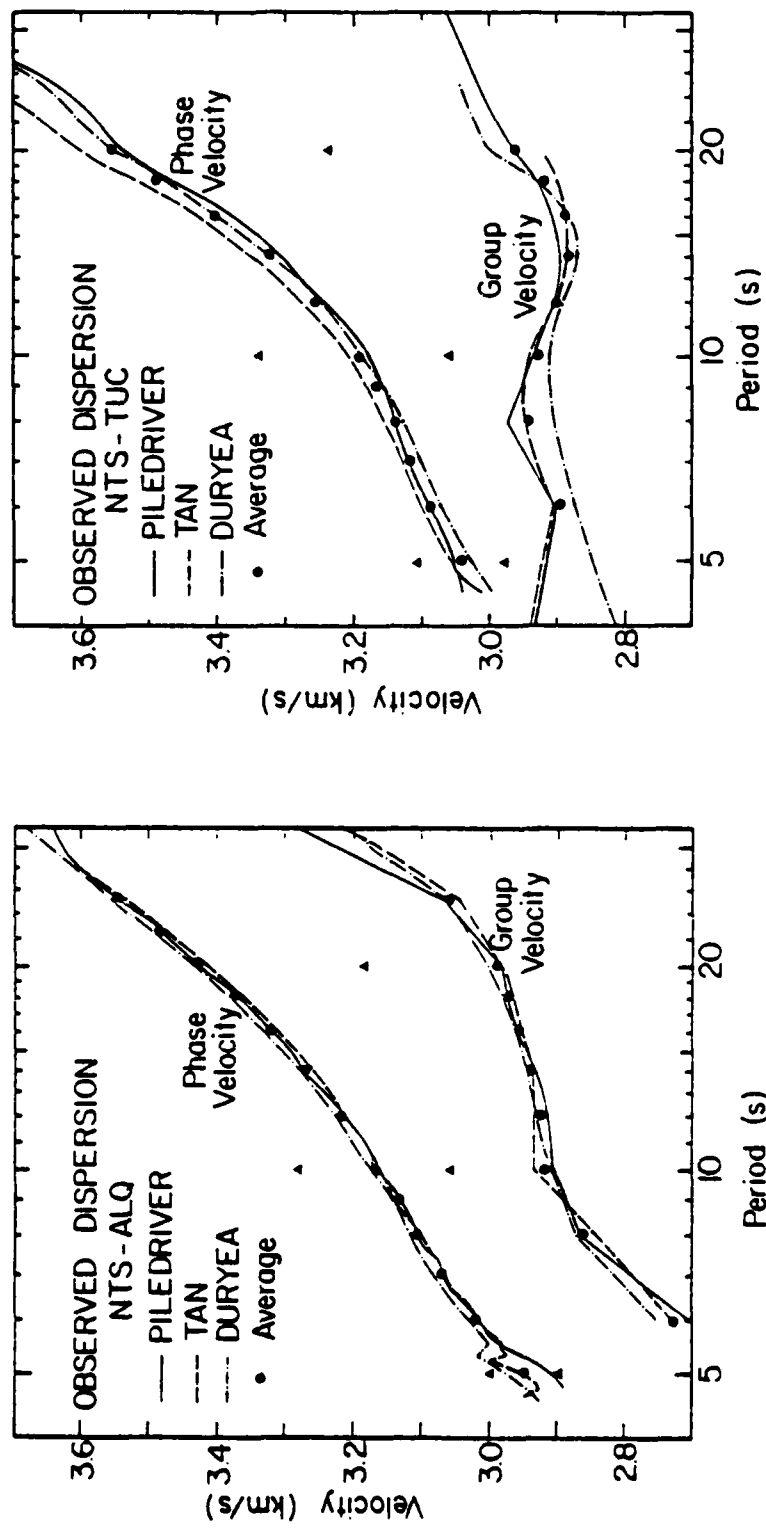


Figure 2. The observed phase and group velocities are shown for three events at NTS to ALQ (left) and TUC (right). The lines denote the values determined from each event, while the closed circles are the average values used in the inversion. The closed triangles are the phase velocities implied by adding plus and minus 2π to the phase spectrum of each seismogram.

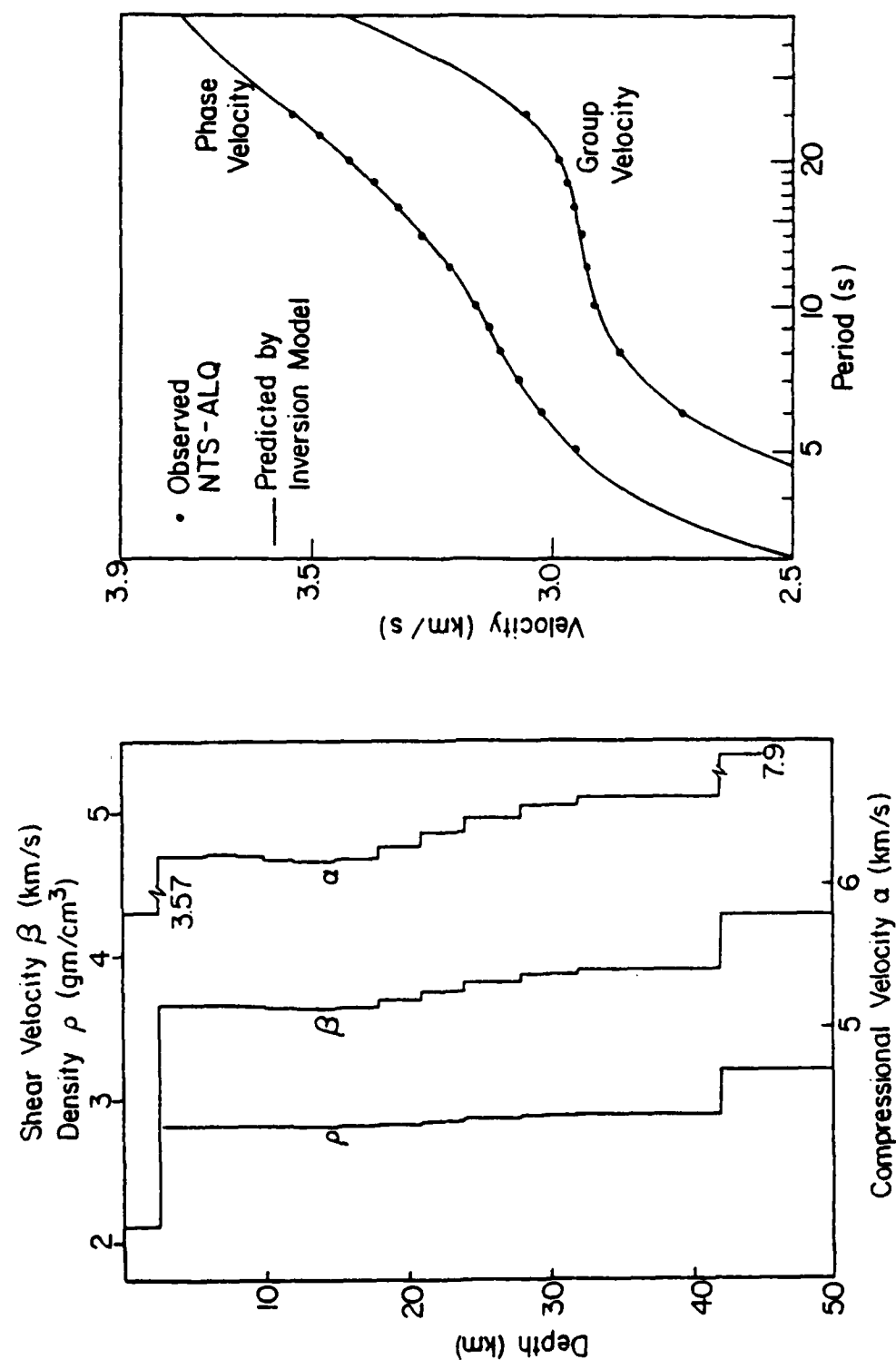


Figure 3. The inversion model (left) for the NTS-ALQ path is shown together with a comparison of its predicted dispersion with the observed NTS-ALQ dispersion.

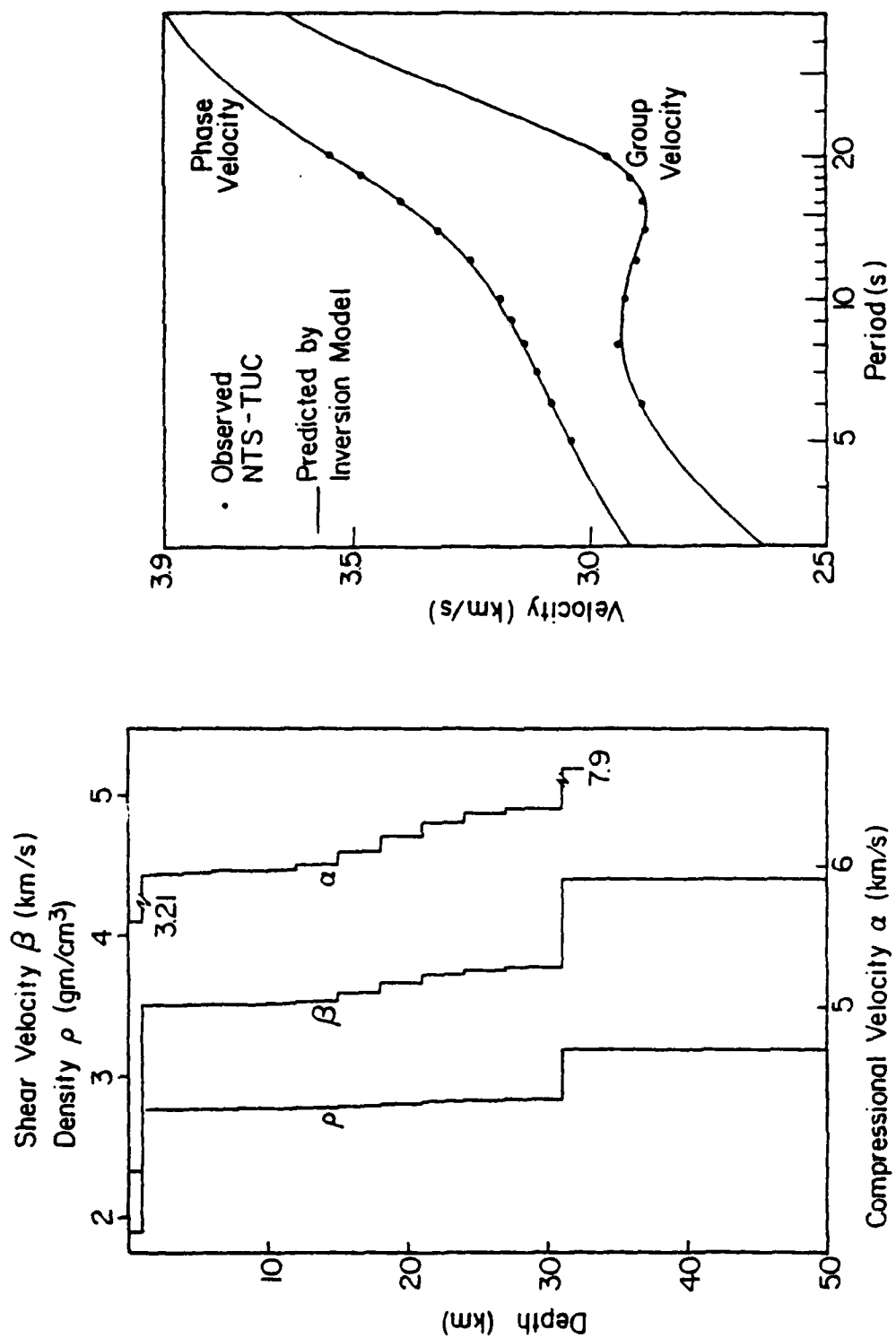


Figure 4. The inversion model (left) for the NTS-TUC path is shown together with a comparison of its predicted dispersion with the observed NTS-TUC dispersion.

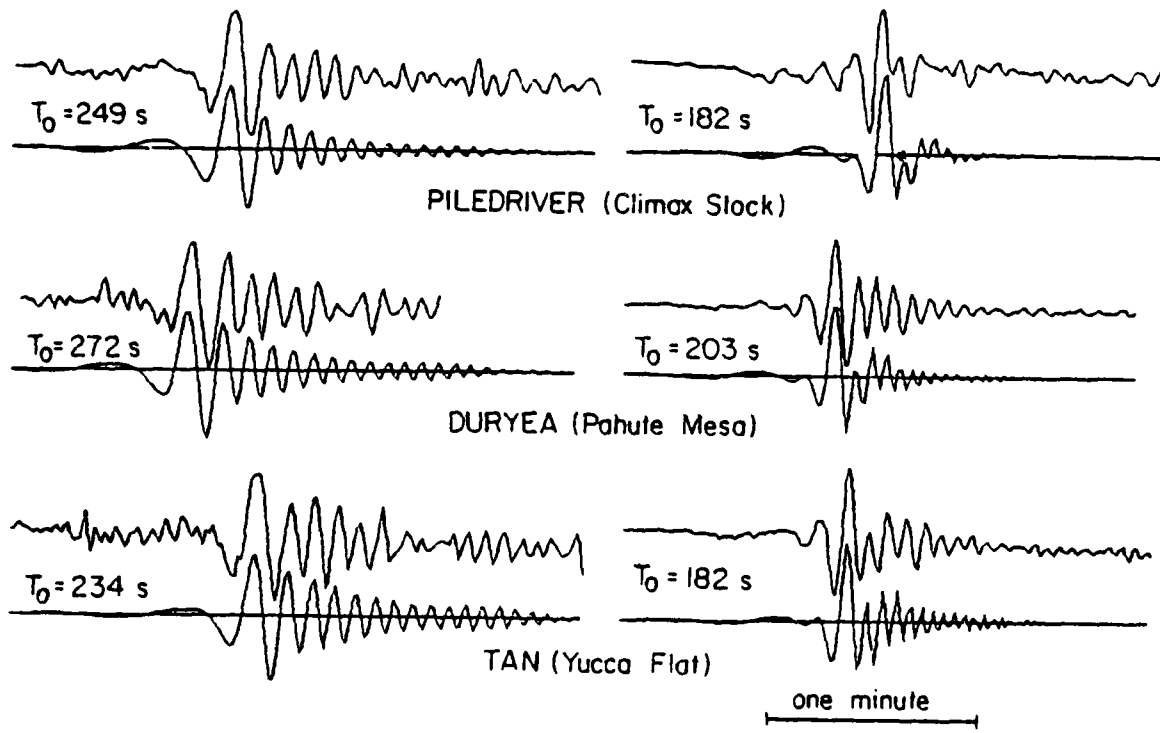


Figure 5. Theoretical and observed seismograms are compared at ALQ (left) and TUC for events in three test areas at NTS. A bar indicating one minute is shown. In each pair the observed (top) and theoretical records start at the same time with respect to the explosion detonation and this time is indicated as T_0 .

The theoretical and observed seismograms agree very well at the two stations, even in some rather subtle details. Agreement of theoretical and observed seismograms requires not only that the dispersion be matched, but that the amplification due to the source and travel path be properly reproduced.

The Airy phase amplitudes and periods can be measured very accurately on the synthetic seismograms. The periods are as follows:

	<u>ALQ</u>	<u>TUC</u>
PILEDRIVER	10.4	8.4
DURYEA	10.7	7.0
TAN	9.9	7.6

These are close to the periods measured (much less accurately) on the observed records which are 11 ± 0.5 seconds for all events at ALQ and 8 ± 0.5 seconds at TUC. The instrument amplification is 0.78 at 7.0 seconds, 0.86 at 8.4 seconds and 0.95 at 10.7 seconds. Therefore, errors in the period measurement do not have much effect on the amplitude determination. In later sections the amplitude comparison will be used to infer the source level.

III. PARAMETRIC DEPENDENCE OF RAYLEIGH WAVE AMPLITUDES

The theoretical relationships used in computing the synthetic seismograms of Figure 5 were given by Bache, Rodi and Harkrider (1978). The basic formula for the vertical component of the fundamental mode Rayleigh wave at range r from a spherically symmetric explosion is

$$\hat{w}(r, \omega) = -4\pi \mu_s \hat{\psi}(\omega) \frac{K_{s_1}^{(h)} A_R}{c_1} T(\omega) H_0^{(2)} \left(\frac{\omega r}{c_2} \right) e^{-\gamma r} \left(\frac{r}{a_e \sin \Delta} \right)^{1/2}, \quad (1)$$

where all quantities are Fourier transformed with respect to time. The μ_s is the shear modulus in the source region, c is Rayleigh phase velocity and $H_0^{(2)}$ is a Hankel function. The A_R is the source depth-independent excitation factor and $K_{s_1}^{(h)}$ is the depth-dependent excitation. The quantity

$$e^{-\gamma r} \left(\frac{r}{a_e \sin \Delta} \right)^{1/2}$$

accounts for anelastic attenuation and the sphericity of the earth.

A two structure model is used for the path with subscript 1 in (1) denoting the source structure and 2 denoting what we call the "path" structure. Note that the dispersion is entirely controlled by the path structure and the amplitude excitation is controlled by the source structure. Passage of Rayleigh waves between the two structures is accounted for by the transmission coefficient $T(\omega)$.

Finally, we have the source which is represented by $\hat{\psi}(\omega)$ in (1). For spherically symmetric explosions this is related to the displacement by

$$\hat{u}(R, \omega) = \left[\frac{\hat{\Psi}(\omega)}{R^2} + \frac{\hat{\dot{\Psi}}(\omega)}{R\alpha} \right] e^{-i\omega R/\alpha}, \quad (2)$$

where R is the range and α is P wave velocity.

We now examine the various factors that control the amplitude of the theoretical seismograms in Figure 5. The source structure was constructed for each of the three examples by altering the top two kilometers of the NTS-TUC path model to represent Pahute Mesa, Yucca Flat or the PILEDRIVER site. The velocity-density profiles for this portion of the models are shown in Figure 6.

From (1), the Rayleigh waves from explosions are proportional to

$$\mu_s \hat{\dot{\Psi}}(\omega) \frac{K_s A_{R_1}}{c_1} T(\omega). \quad (3)$$

For the periods (> 4 seconds) and yields (50-500 KT) of interest, $\hat{\dot{\Psi}}(\omega)$ should be nearly equal to a constant which we call $\hat{\Psi}_\infty$. Our primary objective here is to deduce the value of this $\hat{\Psi}_\infty$.

The source excitation, $\mu_s K_s A_{R_1}/c_1$, and the transmission coefficient, $T(\omega)$, are plotted in Figure 7. We note that $T(\omega)$ is near unity for the periods (≈ 8 seconds for TUC and ≈ 11 seconds for ALQ, see Section II) of primary interest.

The relative source excitation terms for Pahute Mesa and Yucca Flat differ by a nearly constant factor over most of the frequency range. Some of these values and their ratio are given in Table 2. The ratio is little different from the ratio of the shear moduli (μ_s) which is 3.07. This is important because it says that the Rayleigh waves from explosions in the tuffs and rhyolites at Yucca Flat and Pahute Mesa are very nearly proportional to $\mu_s \hat{\dot{\Psi}}(\omega)$.

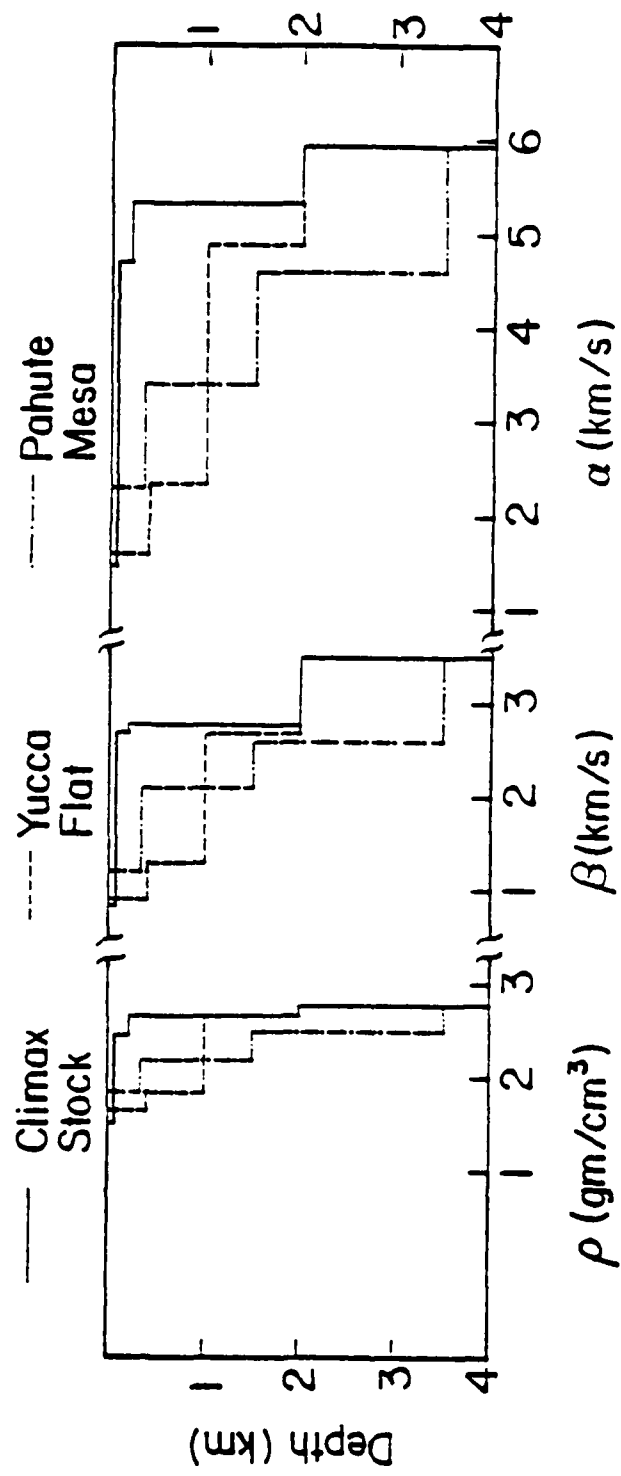


Figure 6. The density and shear and compressional wave velocities are plotted versus depth for the three test areas at NTS. Below 3.5 km the source region models are the same as the NTS-TUC model in Figure 4.

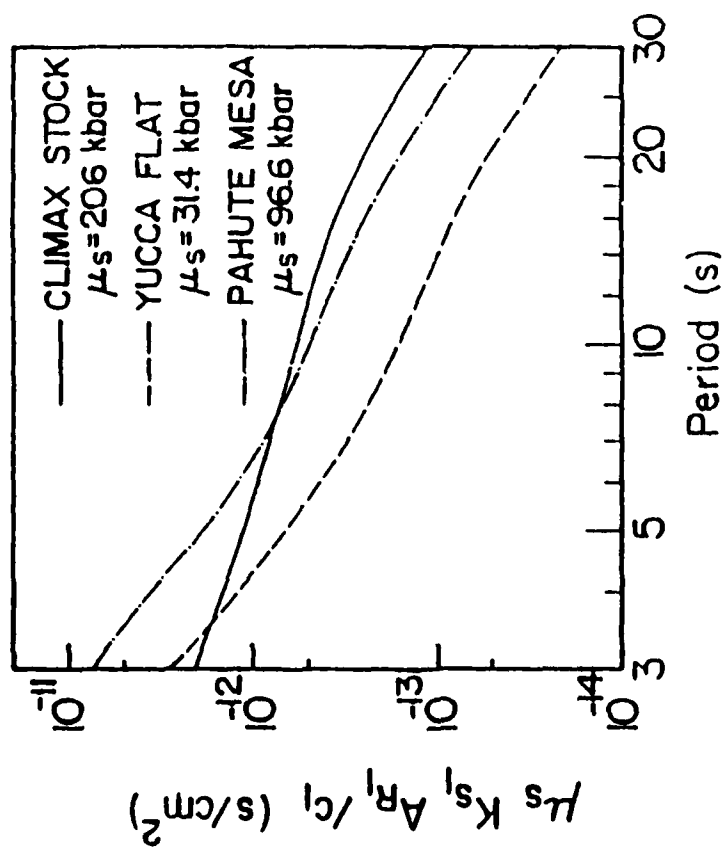
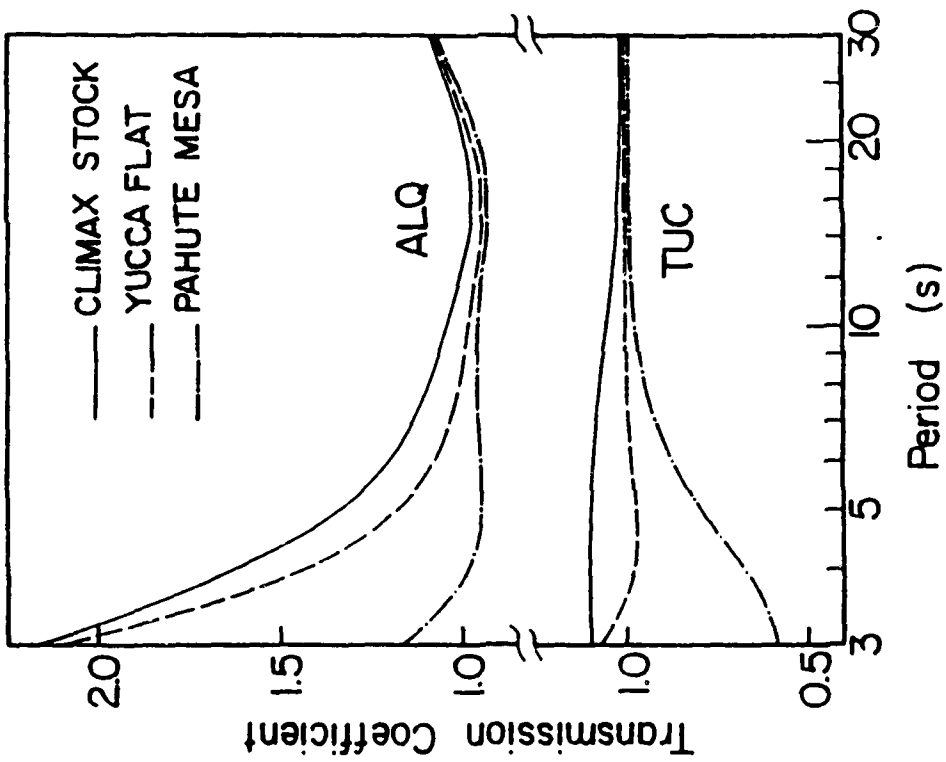


Figure 7. The source excitation factor is shown at left for the three source areas studied. At right is the transmission coefficient $T(\omega)$ for the six source-path combinations.

TABLE 2
VALUES OF THE EXCITATION FACTOR $\mu_s K_{s_1} A_{R_1} / c_1$

<u>Period</u>	<u>Yucca Flat (sec/cm²)</u>	<u>Pahute Mesa (sec/cm²)</u>	<u>Ratio</u>
16	8.11×10^{-14}	2.53×10^{-13}	3.13
14	1.01×10^{-13}	3.12×10^{-13}	3.10
12	1.27×10^{-13}	3.89×10^{-13}	3.06
10	1.68×10^{-13}	5.05×10^{-13}	3.00
8	2.45×10^{-13}	7.14×10^{-13}	2.91
6	4.30×10^{-13}	12.2×10^{-13}	2.83

The PILEDRIVER site, Climax Stock granite, is sufficiently different from the other two that the proportionality to μ_s is not applicable. In fact, the amplitude factor is much smaller than expected from the large μ_s at this site.

The remaining factors in (1) are the Hankel function, which accounts for the dispersion and elastic attenuation, the anelastic attenuation factor $e^{-\gamma r}$ and the sphericity correction. For the ranges of interest, the latter is near unity. The dispersion has a strong effect on the maximum amplitude because it controls the interference between the frequency components.

Our attenuation model for the calculations of Figure 5 is based on Western U. S. data compiled by Mitchell (1975). Since these data were derived from observations of events on the Colorado Plateau, they were assumed to be appropriate for the NTS-ALQ path. Using Mitchell's γ values, we constructed Q models for the two paths, assuming the Q- β relationship was the same for both. These Q models are shown in Figure 8. The $\gamma(\omega)$ which result from these models are tabulated in Table 3. Also shown in Figure 8 are the $e^{-\gamma r}$ for the two paths, using representative distances.

In summary, the factors controlling the maximum peak-to-peak amplitude of the theoretical Rayleigh waves at ALQ and TUC are:

1. The dispersion characteristics of the path model -- from Figure 3 we see that 11 seconds, the period of the maximum phase on the ALQ records, occurs where the group velocity is slowly decreasing. At 8 seconds on the TUC dispersion, Figure 4, the group velocity is near a local maximum. The exact shape of the dispersion curves near the dominant period will influence the amplitude.

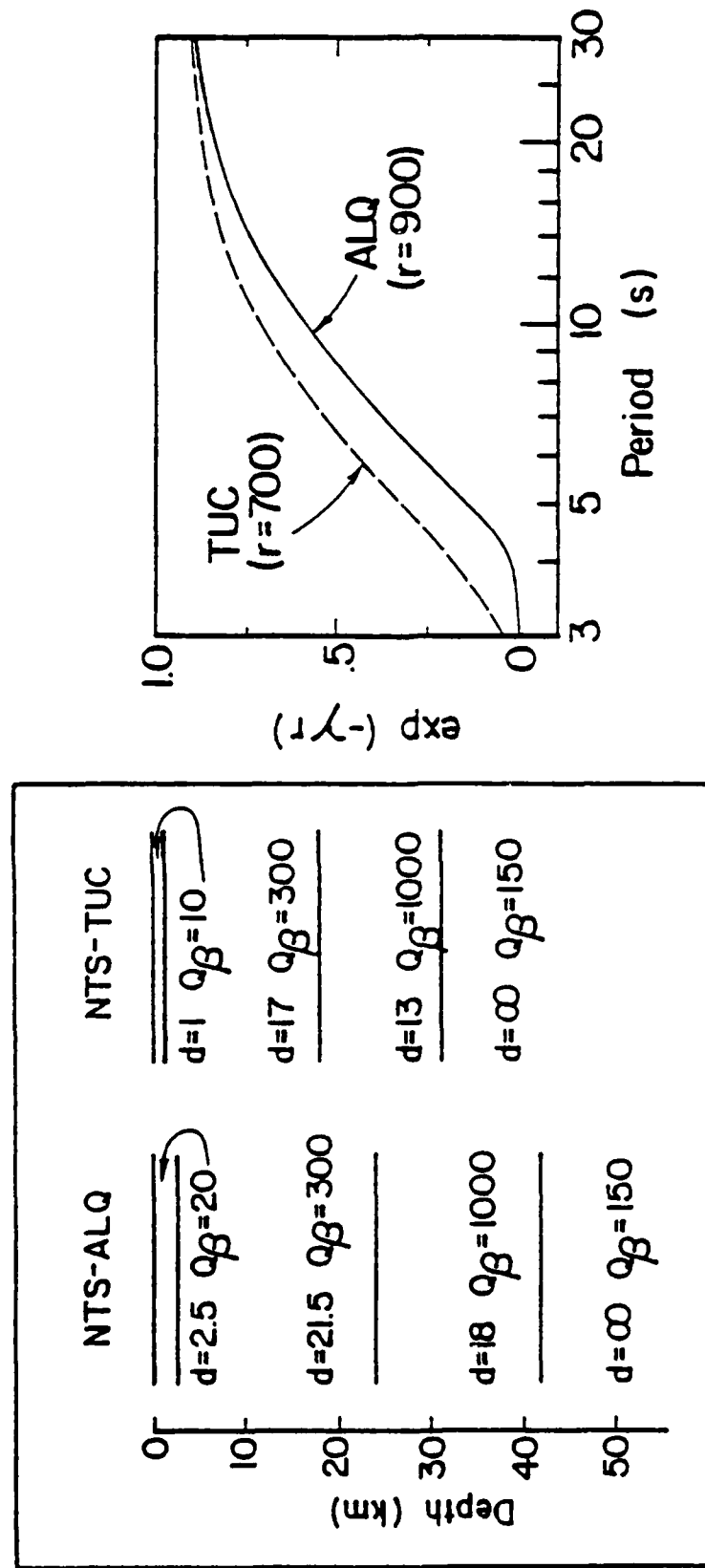


Figure 8. The Q_β models used to derive $\gamma(\omega)$ are shown at left for the NTS-ALQ and NTS-TUC paths with d denoting layer thickness. At the right the amplitude attenuation is plotted for the two paths.

TABLE 3

ATTENUATION PARAMETERS, $\gamma(\omega)$, FOR THE THEORETICAL SEISMOGRAMS OF FIGURE 5

<u>Period</u>	<u>γ, NTS-ALQ</u>	<u>γ, NTS-TUC</u>
25	1.58 ($\times 10^{-4}$ km $^{-1}$)	1.75 ($\times 10^{-4}$ km $^{-1}$)
22.5	1.74	1.89
20	1.96	2.05
18	2.24	2.22
16	2.67	2.47
14	3.33	2.89
12	4.34	3.59
10	5.94	4.80
9	7.12	5.71
8	8.70	6.96
7	11.0	8.74
6	14.5	11.4
5	21.4	15.9
4	43.5	24.2
3	183.0	43.1
2	401.0	114.0

2. The structure in the source region -- this controls the source excitation factors $K_{S1}(h)$, A_{R1} and c_1 . The shear velocity at the source is also a key parameter.
3. The transmission coefficient, $T(\omega)$ -- this quantity accounts for the passage of the Rayleigh wave from the source structure into the path structure.
4. The parameter $\gamma(\omega)$ that accounts for anelastic attenuation and elastic scattering.
5. The source function -- Equation (1) assumes the source is a spherically symmetric explosion. However, the source may include other components. A strong contribution to the Rayleigh waves may be present due to some form of tectonic release (Toksoz and Kehrer, 1972; Lambert, et al., 1972) or spall slapdown (Viecelli, 1973).

Our purpose is to discover the amplitude and nature of the source function. In later sections we will attempt to bound the contribution from the other four factors listed above.

IV. SOURCE ESTIMATES ASSUMING SPHERICAL SYMMETRY

Assuming the source is a spherically symmetric explosion and the path is modeled by the plane-layered earth models described in the previous section, we computed the theoretical seismograms shown in Figure 5. Since the other factors are fixed, the amplitude of the theoretical seismograms can be scaled by the source function, Ψ , in Equation (1). The theoretical seismograms shown in Figure 5 were computed at a depth of 500 meters and a yield of 100 KT using the source function shown in Figure 9. This is source 133 from Bache, et al. (1975) with the frequency axis scaled to 100 KT. This source function was computed for saturated Yucca Flat tuff, but its shape is representative of that deduced in numerous theoretical and empirical studies of NTS explosions.

The amplitude axis in Figure 9 is scaled to 0.02 KT. For any other yield (W) the amplitude is obtained by multiplying by $W/0.02$. Note that the source function is nearly constant over the frequency band of interest. The source level for 5 second waves is about 15 percent larger than for very long period waves. In view of this small deviation from a constant level, it is convenient to characterize the source by Ψ_∞ , the zero frequency limit, which is 10.3 m^3 for 0.02 KT.

In Figures 10 and 11, time-domain Airy-phase amplitudes observed at ALQ and TUC are plotted versus yield for representative events with yields near 100 KT. On each plot, theoretical unit-slope lines indicating constant $\Psi_\infty^{0.02}$ are also shown. The values of $\Psi_\infty^{0.02}$ labeling these lines were determined from the synthetic seismograms in Figure 5. That is, if the $\Psi_\infty^{0.02}$ for the synthetic seismogram calculations had

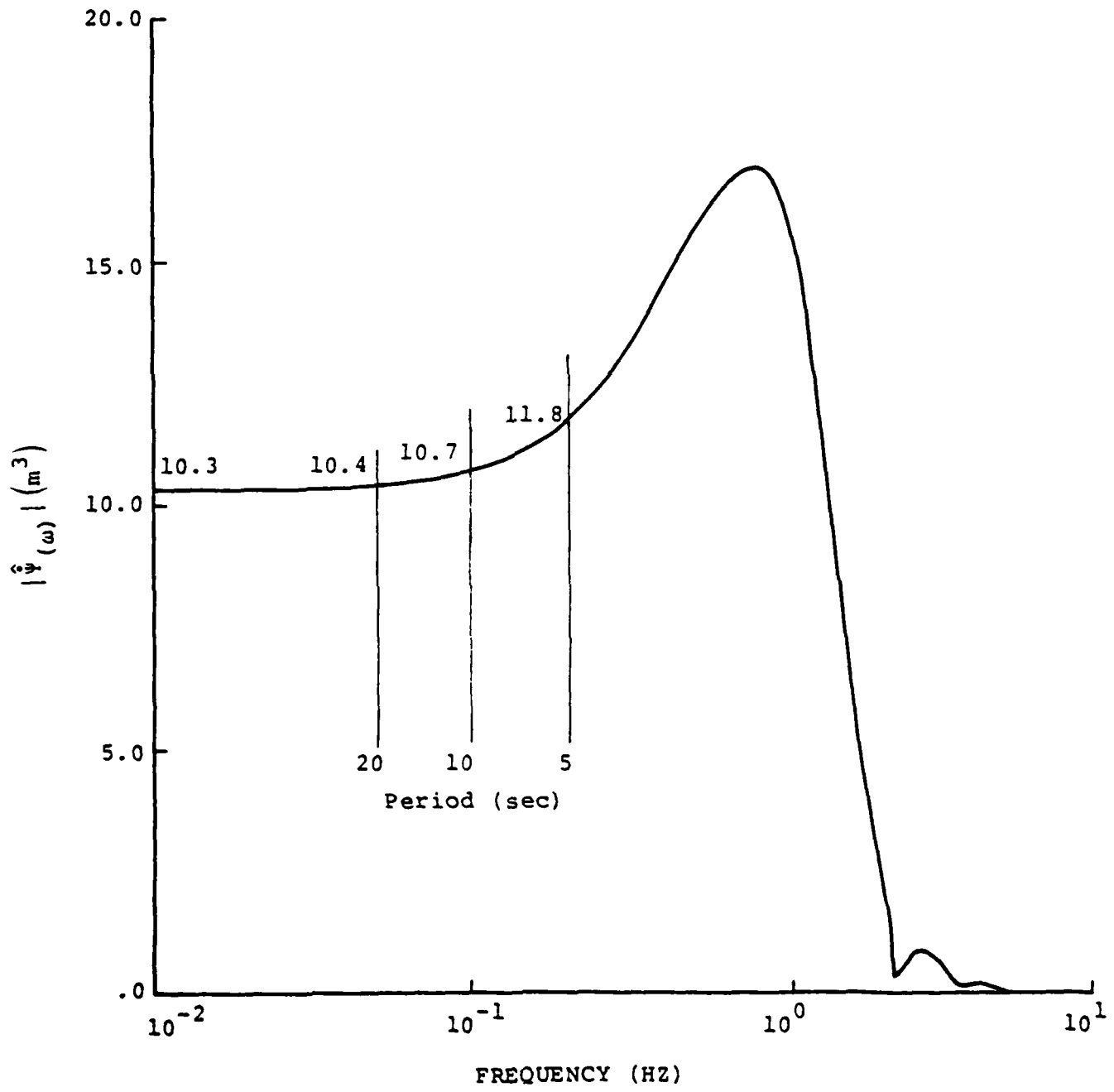


Figure 9. The amplitude of the source function for the theoretical seismograms is plotted with the frequency axis scaled to 100 KT and the amplitude axis to 0.02 KT. The amplitude values at several periods are indicated on the plot.

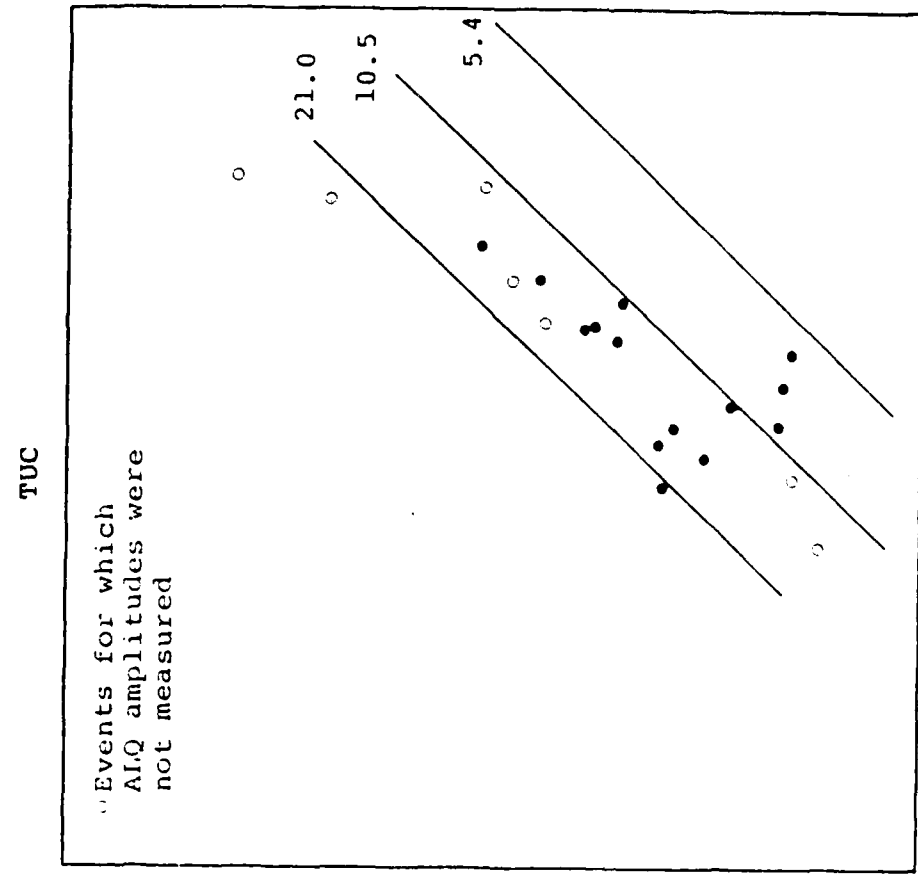
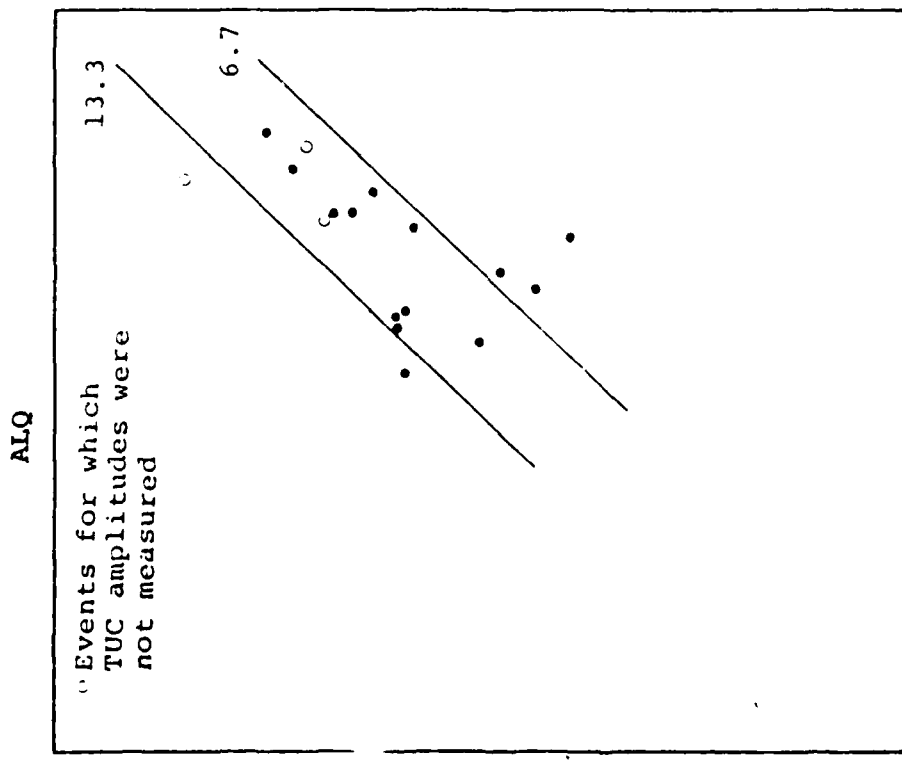


Figure 10. Airy phase amplitudes for Yucca Flat explosions recorded at ALQ and TUC are plotted versus explosion yield. The lines have unit slope.

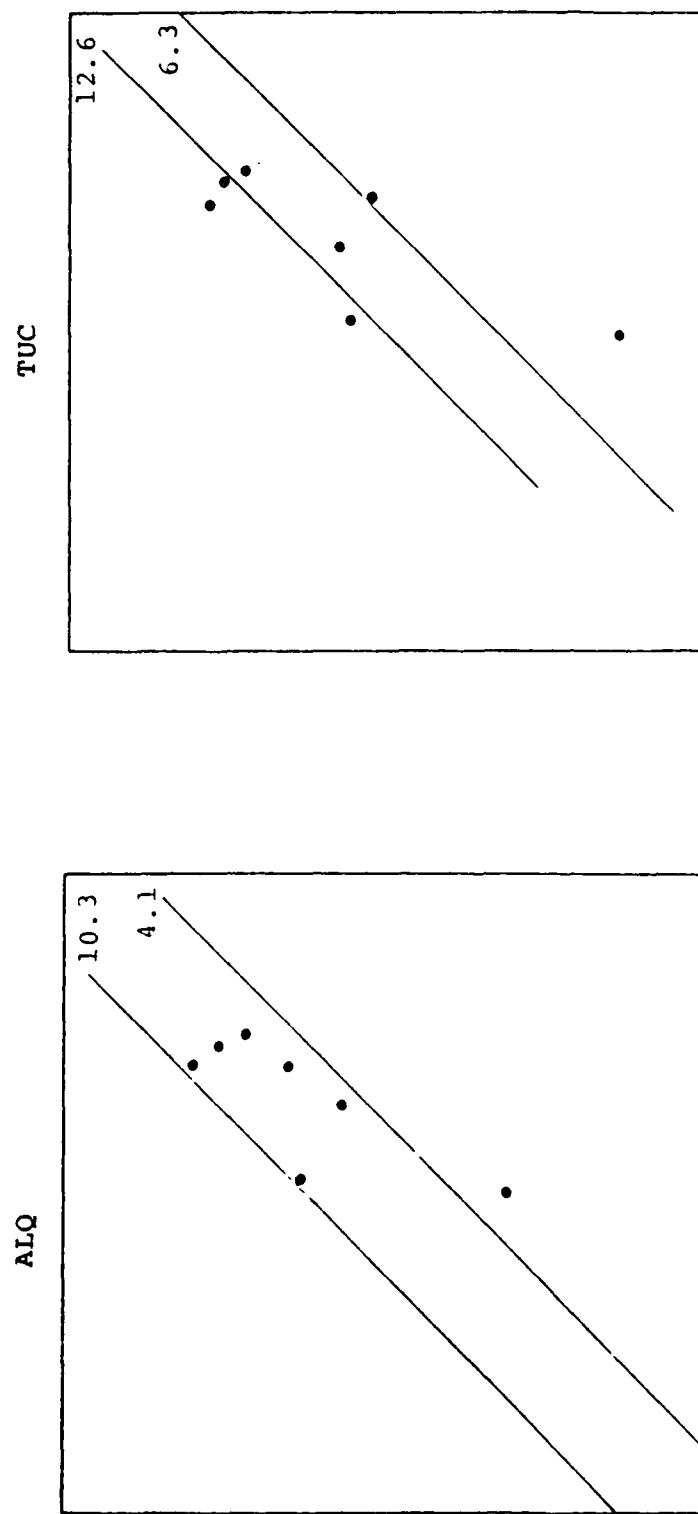


Figure 11. Airy phase amplitudes for Pahute Mesa explosions recorded at ALQ and TUC are plotted versus explosion yield.

these values, then their Airy-phase amplitudes as a function of yield would be described by the lines shown. Neglecting the small correction for the yield scaling of the frequency dependence of $\hat{\Psi}(\omega)$, these lines have unit slope.

The lines in Figures 10 and 11 can be used to deduce the (0.02 KT) source level required to bring theoretical and observed Airy phase amplitudes into coincidence. Note that, on the average, a larger source function seems to be required to fit the TUC data than to fit the ALQ data. We will later discuss this apparent asymmetry at some length. However, we first develop a more quantitative description of the inferred source amplitudes.

Within localized source regions like Pahute Mesa and Yucca Flat, there are several effects that might cause the ratio of Airy phase amplitude to explosion yield to vary from event to event and thus account for the scatter observed in Figures 10 and 11. These include:

1. Range variations,
2. Depth of burial variations,
3. Material rigidity, μ_s , variations
4. Variations in the material properties leading to variations in Ψ_∞/KT .
5. Variations in the frequency dependence of the source function, primarily the ratio of the source level at the Airy phase period, to that at long period.

These items are based on the assumption that the source is spherically symmetric. Asymmetric effects may also cause variations, but we will discuss these later.

We now examine the factors listed above to see what their effects can be. First, for Yucca Flat events, the distance to TUC varies from 708 to 724 km, while for Pahute Mesa events, the TUC range variation is 747 to 764 km. To quantify this effect, synthetic seismograms were computed for the Yucca Flat event TAN at ranges of 708 and 724 km. The amplitude variation was about 8 percent. Similar calculations were done for the Pahute Mesa event DURYEA at 747 and 763.5 km. In this case the Airy phase amplitude variation was less than four percent. In Figure 12 the seismograms at the new distances are compared to the TAN and DURYEA synthetics from Figure 5. We see that the waveforms vary little with small changes in range.

The amplitude variation with depth was determined by comparing theoretical seismograms computed with only the depth changing. For the depths of interest we find the following:

$$\begin{aligned} \text{Yucca Flat: } \log A &\approx 0.16 \log H, \\ \text{Pahute Mesa: } \log A &\approx 0.05 \log H, \end{aligned} \tag{4}$$

where H is the depth of burial. If $H \approx W^{1/3}$, the yield scaling becomes $\log A \approx 1.05 \log W$ for Yucca Flat and $\log A \approx 1.02 \log W$ for Pahute Mesa.

The material rigidity (μ_s) variation can be quite important. As was pointed out in Section III, the Rayleigh wave amplitude is directly proportional to μ_s . Of course, shear modulus variations are likely to be associated with changes in the coupling characteristics of the material; that is, in the $\hat{\Psi}(\omega)$. Such material properties as the water content, air-filled porosity and material strength influence the seismic coupling (Cherry, Rimer and Wray, 1975).

We should also point out that the absolute level of the Ψ_∞ we infer is especially sensitive to the μ_s used in our synthetic seismogram calculations (see Figure 7). Without

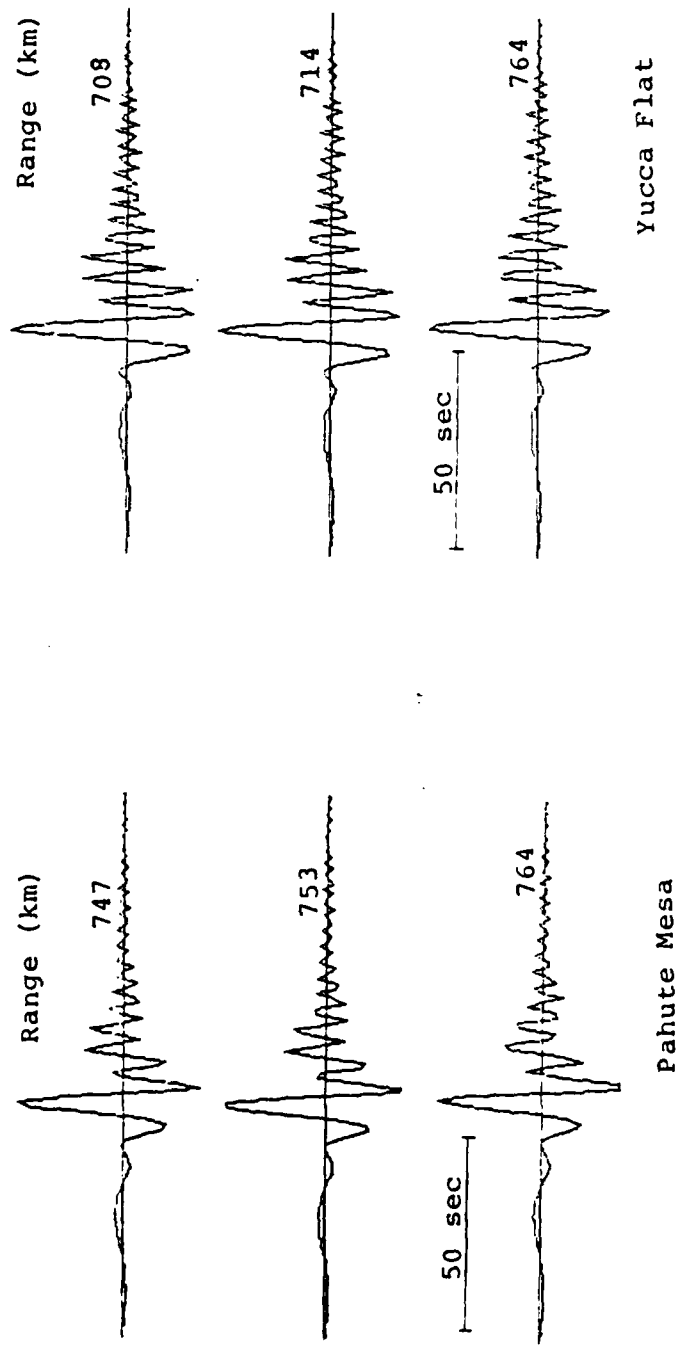


Figure 12. Seismograms are shown at three ranges for two test areas. The middle record in each set is from Figure 5.

independent knowledge of the shear modulus, we can only determine $\mu_s \Psi_\infty$. In subsequent discussion we will continually refer to the inferred Ψ_∞ values, but the trade-off with our assumed μ_s should be kept in mind.

The frequency dependence of the source function, item 5 in the above list, is difficult to quantify. Generally, we would expect the source function to be nearly flat for low yield explosions. However, for very large yields (hundreds of kilotons) the source level at 8 to 10 seconds could be greater than at larger periods.

Estimates of Ψ_∞ were made for each event in the following way. The amplitudes of the synthetic seismograms of Figure 5 were corrected for source depth and yield by multiplying by

$$\left(\frac{H}{500}\right)^n \left(\frac{W}{100}\right), \quad (5)$$

where the n is 0.16 or 0.05 from (4). The small correction for range variations was not made. The event Ψ_∞ values, scaled to 0.02 KT, are then the Ψ_∞ from Figure 9 (10.3) times the ratio of the observed amplitude to the corrected synthetic amplitude. The theoretical source level is a bit higher at the 8 (TUC) and 11 second (ALQ) periods at which the measurements are made, but as long as we realize that the numbers are based on the particular source function shown in Figure 9, this should cause no problem.

The Ψ_∞ were computed from the observations at ALQ and/or TUC for the following events:

Yucca Flat: PIRANHA, BRONZE, GRAPE A, SHAPER, TAN
MINATA, STARWORT, CUP, CALABASH, OSCURO,
GRAPE B, LAMPER, NOGGIN, DUMONT, BUFF,
MIERA, AGILE, CORDUROY, TIJERAS, ZAZA
and KNOX;

Pahute Mesa: DURYEA, KNICKERBOCKER, CHATEAUGAY,
SCOTCH, STINGER, PURSE, SLED;
PILEDRIVER.

The inferred $\Psi_{\infty}^{.02}$ values are plotted versus explosion yield in log-log form in Figure 13. For each population the logarithmic mean values and their 95 percent confidence limits were computed using Student's t distribution. These values are shown on the plot and are summarized in Table 4. If the source were spherically, or at least axially, symmetric and our theory properly accounted for the path, the Ψ_{∞} estimates would be the same at ALQ and TUC for each event. However, the source level required to match the TUC amplitudes appears to be significantly larger than that required to match the ALQ amplitudes.

Since our data span only a narrow yield range, we are unable to determine the dependence of the Ψ_{∞} values on yield (or depth of burial, since the two are nearly proportional). This is demonstrated in Table 5 by the results of a linear regression fit to the data plotted in Figure 13. If cube-root scaling applies, the true Ψ_{∞} is proportional to W and the slope of $\Psi_{\infty}^{.02}$ versus W would be zero. For all four sets the slope is negative suggesting that $\Psi_{\infty} \approx W^n$ with $n < 1$. However, the confidence limits are quite wide and we can have little confidence that the slope is different from zero (or other values near zero that might be thought appropriate).

How much of the scatter in the source estimates is real, that is, associated with real differences in the source amplitude per kiloton of yield? The standard deviations in Table 4 are about 35 to 45 percent of the mean. The yield is only determined to within about ± 15 percent and this accounts for some of the scatter. From the WWSSN film it is generally not possible to measure the amplitudes any closer than within 5 to 10 percent (we know that range differences add errors of a few percent). Also, the instrument gain may vary with time and not be the same as the assumed values. This could add errors of at least several percent. Therefore, if we

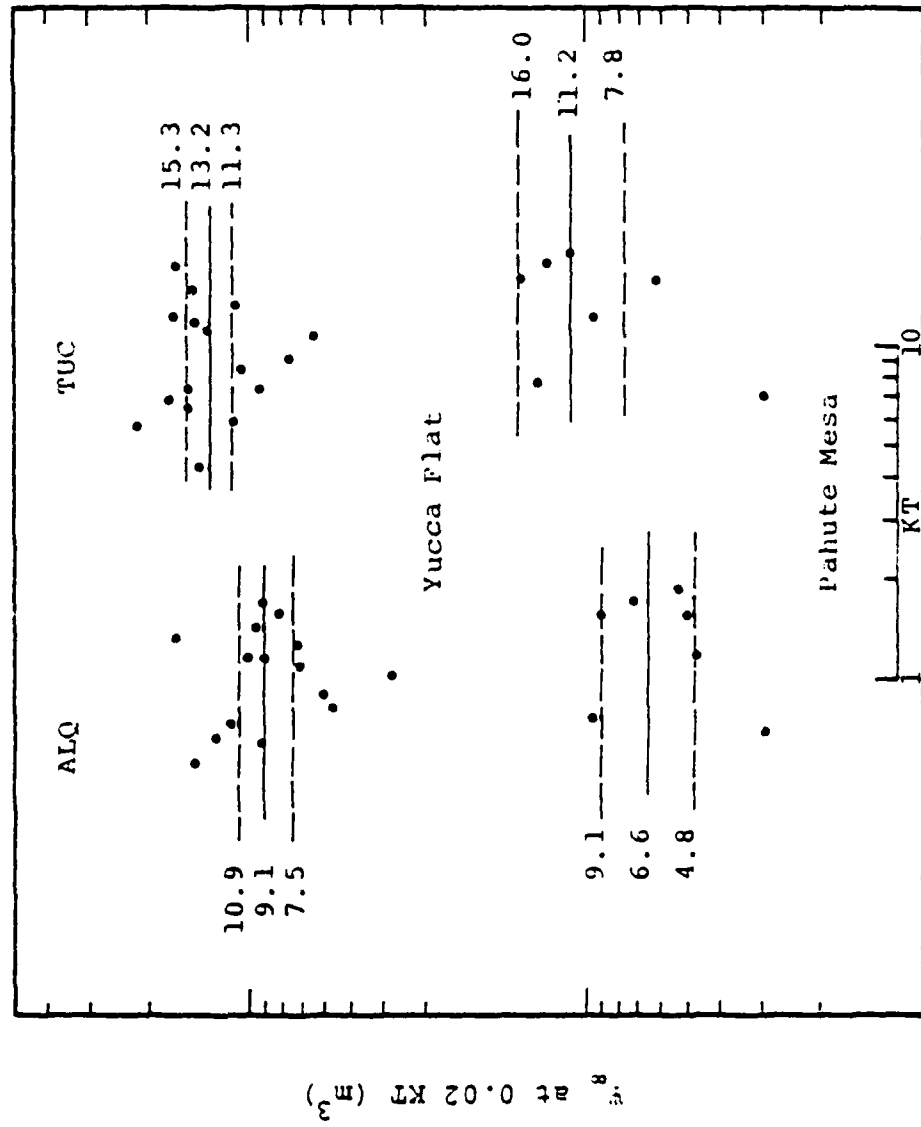


Figure 13. The Ψ_∞ values (at 0.02 KT) are plotted versus explosion yield for the Yucca Flat and Pahute Mesa events. The plot is log-log and the mean and 95 percent confidence limits on the mean are shown. One decade of yield is shown for reference.

TABLE 4
INFERRED VALUES OF Ψ_∞ SCALED TO 0.02 KT

<u>Events</u>	<u>ALQ Ψ_∞</u>	<u>TUC Ψ_∞</u>	<u>Ψ_∞ (TUC)</u>
			<u>Ψ_∞ (ALQ)</u>
Yucca Flat	9.1	13.2	1.50
95% confidence limits	7.5 - 10.9	11.3 - 15.3	1.32 - 1.69
Standard deviation [†]	44%	35%	24%
	n = 17	n = 18	n = 14
Pahute Mesa	6.6*	11.2*	1.57
95% confidence limits	4.8 - 9.1	7.8 - 16.0	1.22 - 2.03
Standard deviation [†]	36%	40%	31%
	n = 6	n = 6	n = 7
PILEDRIVER	3.9	6.2	1.59

* Deleting one event known to be above the water table and therefore likely to have lower coupling.

[†] The standard deviation is given as a percentage of the mean.

TABLE 5
LINEAR REGRESSION FIT TO THE INFERRED Ψ_∞ DATA

Events	<u>ALO</u>	<u>TUC</u>
Yucca Flat	$\log \Psi_\infty \approx -.21 \log W$	$\log \Psi_\infty \approx -.02 \log W$
95% confidence limits on slope	± 0.6	± 0.4
Pahute Mesa	$\log \Psi_\infty \approx -.41 \log W$	$\log \Psi_\infty \approx -.21 \log W$
95% confidence limits on slope	± 1.2	± 1.4

assume these random effects are independent of one another, they account for less than half of the scatter. We also expect some real source amplitude differences due to variations in μ_s and other source region material properties. Any non-axisymmetric effects that are present may also cause variations in the apparent source amplitude.

In summary, we have assumed the source was a spherically symmetric explosion characterized by the reduced velocity potential shown in Figure 9. Correcting for the burial depth and yield according to (5), we estimated the Ψ_∞ required to match the data for each event. Mean values were computed for the Yucca Flat and Pahute Mesa events at each station. The standard deviations are about 35-45 percent of the mean. Scatter of at most half this magnitude is expected from the presence of random errors in the yield estimates and amplitude measurements. Real variations in the Ψ_∞ for each population are therefore thought to have standard deviations exceeding 20 percent of the mean.

There are several features of the Ψ_∞ estimates that require further discussion. First, there is the significance of these values in view of nonspherical effects such as tectonic release and spall slapdown that are widely believed to influence Rayleigh wave generation. Second, there is the asymmetry in the source estimates from the two stations. Finally, there are the relative values for the three test areas. The ratio of the mean Pahute Mesa Ψ_∞ to that from Yucca Flat is 0.73 at ALQ and 0.85 at TUC. These values are consistent, though the confidence limits show that we cannot be certain that the lower Ψ_∞ for Pahute Mesa is meaningful. Comparing PILEDRIVER to Yucca Flat, the Ψ_∞ ratios are 0.43 for ALQ and 0.47 for TUC. Again, the values are remarkably consistent. Within the limits imposed by the statistics, the relative source levels appear to be well determined by the procedure we have used, though we should keep in mind that it is the relative $\mu_s \Psi_\infty$ that is being determined.

The absolute source levels are consistent with those computed using deterministic models for the constitutive behavior of the NTS granite, tuff and rhyolite. For example, in Figure 14 we show computed source function spectral amplitudes, $|\hat{\Psi}(\omega)|$, for several NTS materials. These source functions are from Bache, *et al.*, (1975), and are consistent with the relative amplitudes of teleseismic body waves which are sensitive to the source function amplitude near 1 Hz. Varying the air-filled porosity (ϕ_0) of the Yucca Flat tuff, we get the source functions shown in Figure 15. This figure includes the source 133 used in our synthetic seismogram calculations. The effect on the Pahute Mesa rhyolite source of varying the crush pressure, P_c , is shown in Figure 16. The P_c is the pressure at which the air-filled voids are irreversibly removed from the rock.

In Figure 17 we show the spectral amplitude of the analytical form for observed source functions given by Haskell (1967). The "observed" source functions were computed by Werth and Herbst (1963) from ground motion measurements in the vicinity of several low yield events. Another example is given in Figure 18 where the PILEDRIVER source function 130 is compared to source functions computed from radial velocity records obtained at stations at two horizontal ranges (Perret, 1968).

The theoretical and observed Ψ_∞ values from Figures 14 - 18 are compared to those inferred in this study in Table 6. All values are in meters cubed and scaled to 0.02 KT. Clearly our inferred values are about the right size. For Yucca Flat tuff the theoretical source with low (1.6 percent) air-filled porosity, source 133, is in good agreement with the observed values. The questionable value for the observed tuff Ψ_∞ is from the RAINIER event and the material properties were probably significantly different than for the events we studied. For Pahute Mesa the theoretical values may be a little small, but the agreement with the values we inferred

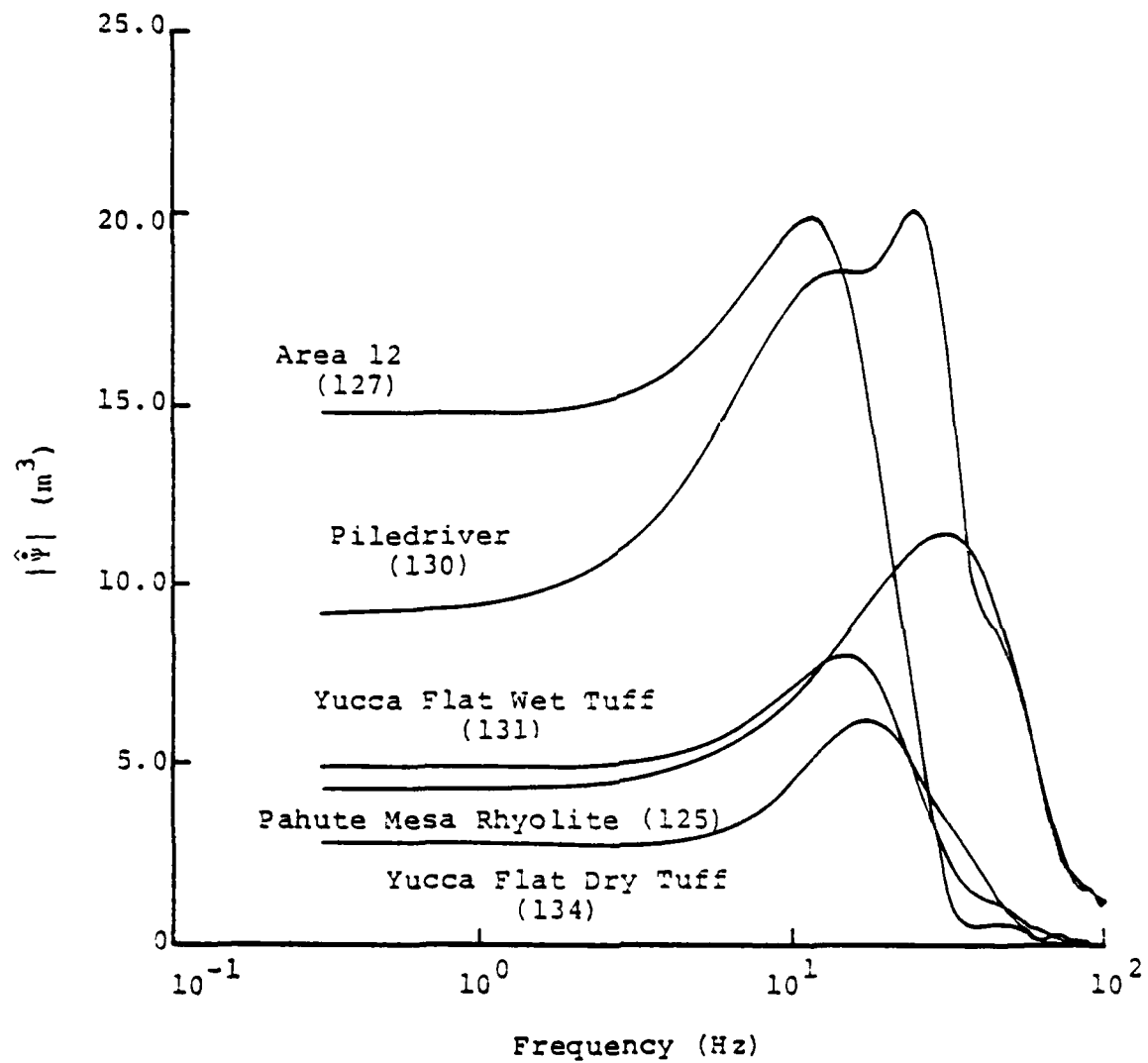


Figure 14. Source spectra scaled to 0.02 KT are shown for the indicated materials.

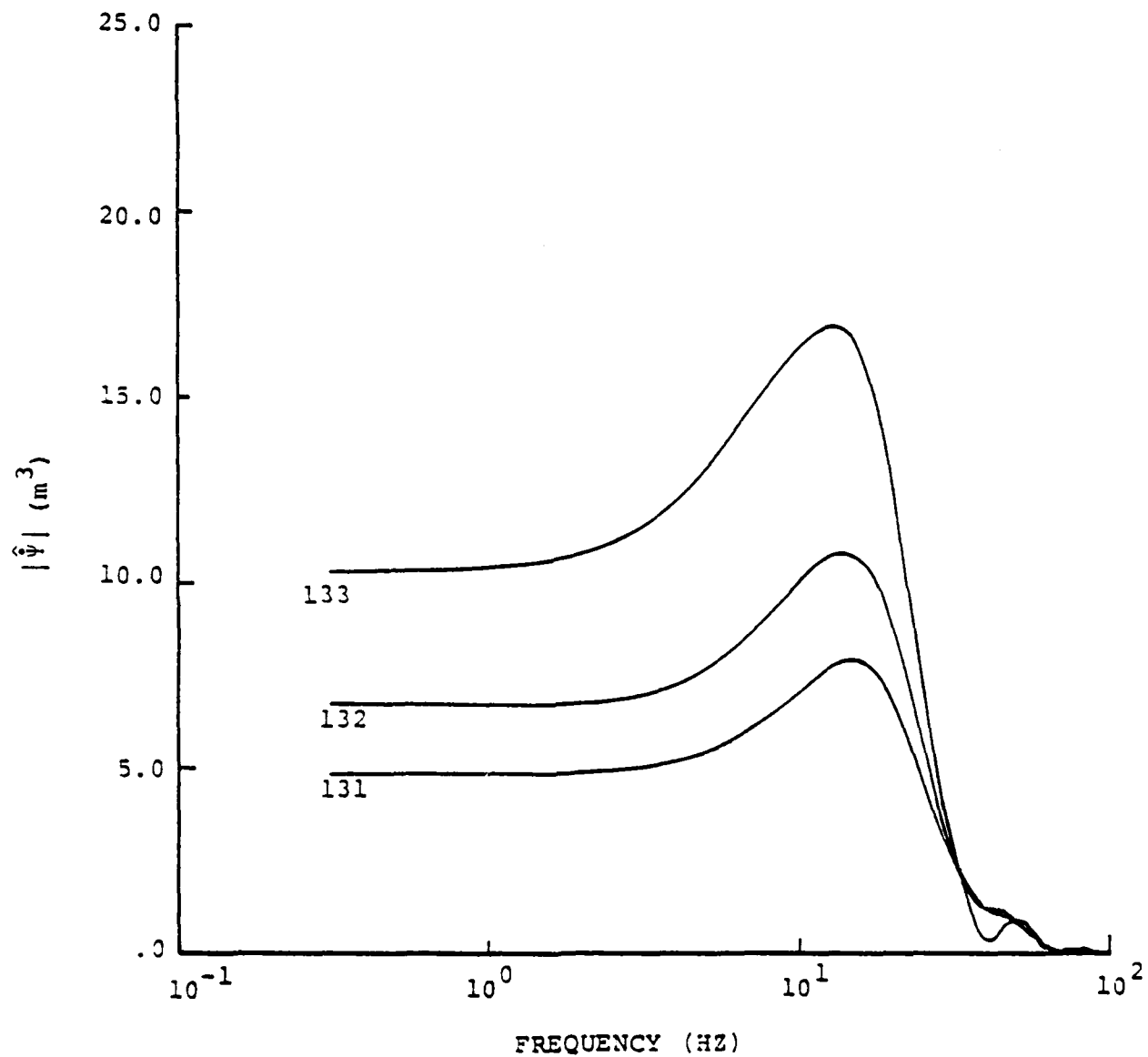


Figure 15. Source spectra scaled to 0.02 KT are shown for calculations 131 ($\phi_0 = 4.4$ percent), 132 ($\phi_0 = 3.0$ percent) and 133 ($\phi_0 = 1.6$ percent) for Yucca Flat wet tuff.

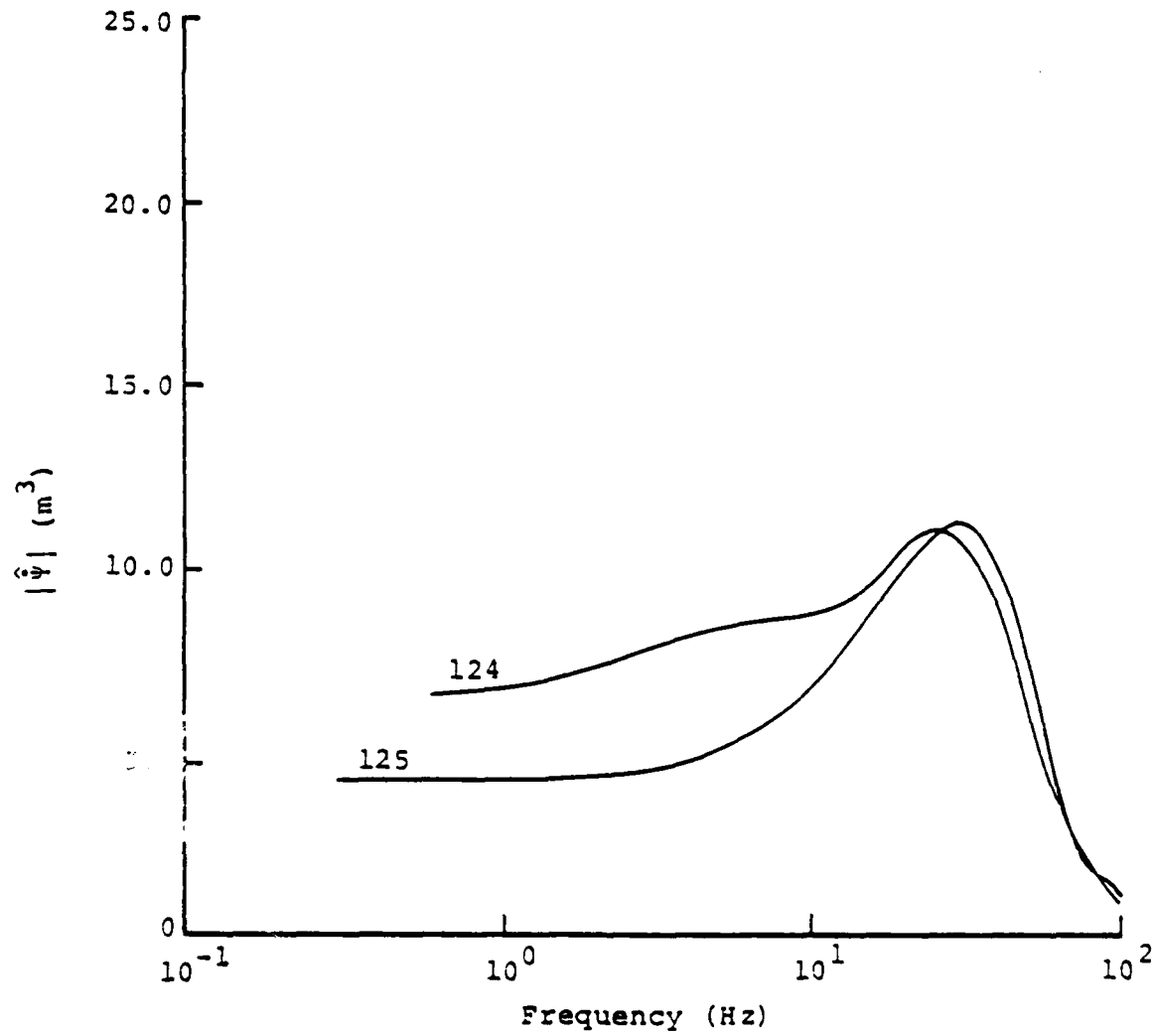


Figure 16. Source spectra scaled to 0.02 KT are shown for calculations 124 ($P_c = 0.5$) and 125 ($P_c = 1.0$) in Pahute Mesa rhyolite.

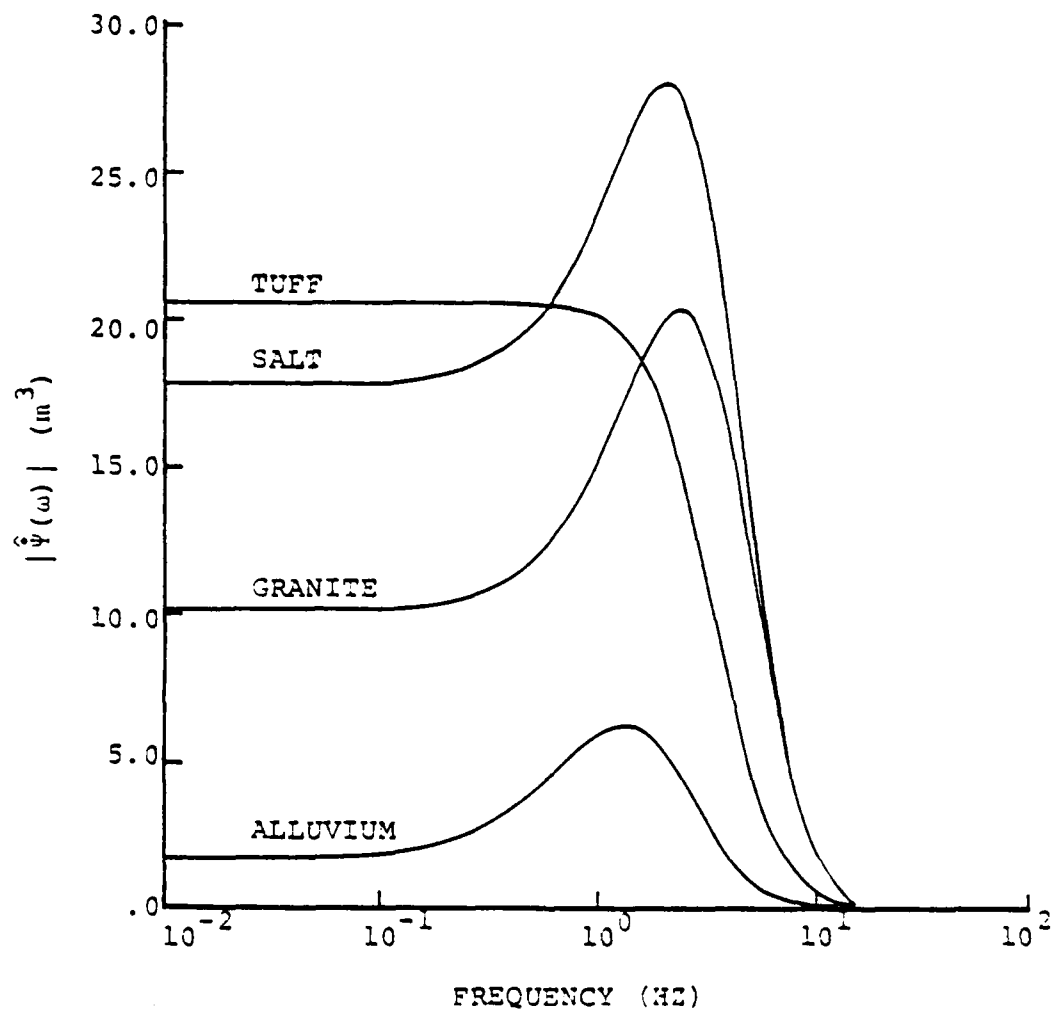


Figure 17. The analytical source functions calculated by Haskell (1967) from data given by Werth and Herbst (1963) are shown with the amplitudes scaled to 0.02 KT and the frequency axis scaled to 5 KT.

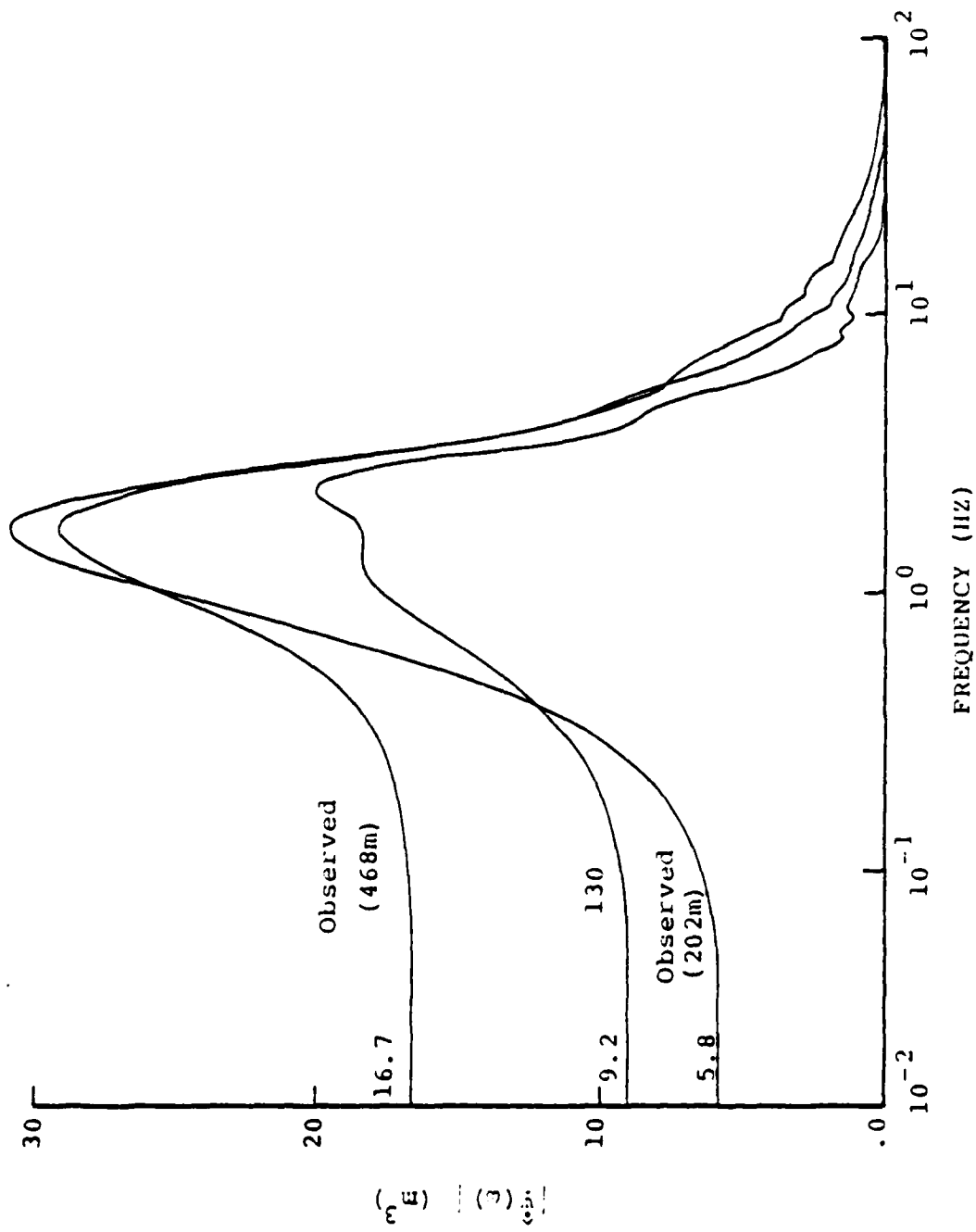


Figure 18. The source function amplitudes computed from PILEDRIVER observed velocity records at two ranges are compared to the theoretical source 130. The amplitude axis is scaled to $0.02 K_T$.

is quite acceptable. Finally, for PILEDRIVER the inferred Ψ_∞ values are significantly smaller than the observed granite values from two events (Haskell's value is for HARDHAT) or for the theoretical value which was computed to simultaneously match the near-field and teleseismic short period data. The reason for this discrepancy is not clear at this time, but it is not obvious which values are more nearly correct.

Another interesting comparison is to the Ψ_∞ values inferred from the seismic moments computed by Tsai and Aki (1971) and summarized by Aki, et al. (1974). The moment, M_0 , is related to Ψ_∞ by

$$M_0 = 4\pi\rho\alpha^2 \Psi_\infty . \quad (6)$$

The P wave velocity, density and shear modulus for our determination of Ψ_∞ are (Figures 6 and 7):

Yucca Flat: $\alpha = 2.35$, $\rho = 1.86$, $\mu_s = 31.4$

Pahute Mesa: $\alpha = 3.4$, $\rho = 2.19$, $\mu_s = 96.6$

PILEDRIVER: $\alpha = 5.33$, $\rho = 2.67$, $\mu_s = 206.$

Aki, et al. (1974) list seismic moments for eight Yucca Flat (MONERO, BUFF, PIRANHA, BRONZE, TAN, OSCURO, CORDUROY and DUMONT) and four Pahute Mesa (KNICKERBOCKER, HALFBEAK, BENHAM and BOXCAR) events as well as PILEDRIVER. Using (6) the Ψ_∞ values were computed for each of these events and scaled to 0.02 KT. The logarithmic mean values for each population are listed in Table 6 along with their 95% confidence limits.

The moment calculations of Tsai and Aki (1971) were based on ALQ recordings for all events except BOXCAR and BENHAM where recordings from Spring Hill, Alabama were used. The Ψ_∞ values obtained from the moment are slightly smaller than ours for PILEDRIVER and somewhat larger than our average Ψ_∞ for the other two populations. In view of the differences in the methods for correcting for the travel path, we would not expect much better agreement.

Another way to estimate Ψ_∞ was suggested by Murphy (1974) in a discussion of the paper by Aki, et al. (1974). He points out that for incompressible materials

$$\Psi_\infty = R_C^3/3 , \quad (7)$$

where R_C is the cavity radius. Using an empirical relationship between cavity radius, depth and yield derived by Orphal (1970) for explosions in tuff, he finds that

$$\Psi_\infty = 1190 W^{0.89} m^3 . \quad (8)$$

The values computed from (8) are summarized in Table 6. From a theoretical point of view, Equation (7) provides an upper limit for the actual Ψ_∞ . For the calculations leading to the theoretical source functions shown in Figures 14 - 16, the ratio of $R_C^3/3$ to Ψ_∞ is 1.2 - 1.8 for the granite and rhyolites, 5 to 14 for the saturated tuffs and about 18 for the dry, porous tuff. Taking these factors into account, the values inferred from the cavity radii suggest that our inferred Ψ_∞ are, perhaps, a little too large.

In summary, we have estimated the Ψ_∞ for three classes of events, assuming the source is spherically symmetric. For Yucca Flat and Pahute Mesa the theoretical results, which were developed to match the teleseismic short period body waves, tend to support the smaller of the two estimates, that from the ALQ data. The values inferred from the cavity radius also support the ALQ estimates. (These two estimates are not entirely independent since the theoretical calculations took cavity radius into account). The Ψ_∞ values inferred from the moment are larger than our values, but this is likely to be due to the different path correction used by Tsai and Aki (1971).

TABLE 6

COMPARISON OF THEORETICAL AND OBSERVED Ψ_∞ VALUES TO THOSE
INFERRRED FROM THE ALQ AND TUC RAYLEIGH WAVES. ALL
 Ψ_∞ VALUES ARE SCALED TO 0.02 KT.

	<u>Yucca Flat</u>	<u>Pahute Mesa</u>	<u>PILEDRIVER</u>
ALQ Inferred	9.1 7.5 - 10.9 n = 17	6.9 4.8 - 9.1 n = 6	3.9
TUC Inferred	13.2 11.3 - 15.3 n = 18	11.2 7.8 - 16.0 n = 6	6.2
Inferred from moment values of Aki, <u>et al.</u> , 1974	16.6 13.2 - 20.7 n = 8	16.2 12.5 - 21.0 n = 4	3.75 [†]
Inferred from cavity radius (Murphy, 1974)	15.1 13.8 - 16.6 n = 8	12.2 9.6 - 15.3 n = 4	-
Theoretical			
Figure 14	4.8	4.2	9.2
Figures 15 & 16	6.8, 10.3	7.2	-
Observed			
Figure 17	20.5*	-	10.0
Figure 18	-	-	5.8, 16.7

* Haskell (1967) lists this value as questionable.

[†] Based on a yield of 56 KT.

For PILEDRIVER the inferred Ψ_∞ value is substantially smaller than the theoretical value and that obtained from integrated velocity recordings. However, in this case, the estimate from the moment is smaller than our Ψ_∞ derived from either ALQ or TUC.

We know that explosions deviate substantially from spherical symmetry. In the next section we study the influence on our solution of some plausible nonspherical effects. Another important aspect of our solution is the difference between the source estimates from the two stations. This will be discussed in Section VII.

V. CORRECTION FOR THE EFFECT OF A DOUBLE-COUPLE ENHANCEMENT OF THE SOURCE

Two often observed and discussed phenomena that are incompatible with the assumption of spherical symmetry for underground nuclear explosions are surface spall and tectonic strain release. In the next two sections we estimate the effect these phenomena might have on our source estimates.

The evidence for explosions being accompanied by a double-couple generated by some type of tectonic strain release is quite convincing (Töksöz, et al., 1971; Lambert, et al., 1972; Aki and Tsai, 1972). Töksöz and Kehrer (1972) inferred the size of the double-couple associated with several of the events studied here. Assuming a vertical strike-slip orientation, the Rayleigh waves from the composite source made up of the explosion plus the double-couple may be written

$$w_t = w_e (1 + F \sin 2\theta) , \quad (9)$$

where w_t and w_e are the total and explosion generated Rayleigh wave amplitudes. The F represents the size of the double-couple relative to the explosion and θ is the azimuth from the strike. Using the F and θ given by Töksöz and Kehrer (1972), the w_t were computed for several events and are tabulated in Table 7. Also tabulated are the TUC/ALQ ratios. These indicate the relative size of the source as viewed from TUC compared to its size when viewed from ALQ. For the Yucca Flat and Pahute Mesa events the double-couple radiation pattern tends to make the source look bigger at TUC. If the population of events in Table 7 is a random sample, we could conclude that the source appears to be something like 5 to 30 percent larger at TUC due to the tectonic release radiation pattern. This would explain part of the difference in the Ψ_∞ estimates from ALQ and TUC in Table 4. However, the inferred radiation pattern for PILEDRIVER tends to slightly increase the ALQ-TUC Ψ_∞ asymmetry.

TABLE 7

CORRECTION OF THE RAYLEIGH WAVE AMPLITUDES FOR THE DOUBLE-COUPLE
SOLUTION OF TOKSÖZ AND KEHRER (1972)

EVENT	F	θ	TUC w_t/w_e	ALQ w_t/w_e	$\frac{w_t(\text{TUC})}{w_t(\text{ALQ})}$
Yucca Flat					
CUP	.55	20°	1.43	.87	1.64
TAN	.39	347°	1.34	1.31	1.02
BRONZE	.33	5°	1.33	1.09	1.22
BUFF	.31	28°	1.18	.76	1.55
CORDUROY	.72	347°	1.64	1.57	1.05
BILBY*	.47	340°	1.35	1.43	.94
HAYMAKER*	.33	340°	1.25	1.30	<u>.96</u>
Mean \pm one standard deviation $1.36 \pm .15$ $1.19 \pm .30$ $1.20 \pm .29$					
Pahute Mesa					
DURYEA	.75	355°	1.74	1.44	1.21
CHARTREUSE*	.90	353°	1.87	1.58	1.18
HALFBEAK*	.67	345°	1.58	1.56	1.01
BENHAM*	.85	345°	1.74	1.71	1.02
BOXCAR*	.59	346°	1.52	1.48	1.03
GREELEY*	1.6	355°	2.58	1.94	<u>1.33</u>
Mean \pm one standard deviation $1.84 \pm .38$ $1.62 \pm .18$ $1.13 \pm .13$					
PILEDRIVER	3.2	340°	3.00†	3.55†	.85

*Events not included in the population observed at ALQ and/or TUC

†These values are based on synthetic seismogram calculations. They are about 10 percent smaller than those obtained from Equation (9) due mainly to the source amplitude being slightly different at the measurement period than at zero frequency.

From the values in Table 7 we conclude that the double-couple component increases the Rayleigh waves at ALQ and TUC in most cases. If we correct for this effect, our estimate of the Ψ_∞ for the explosion is reduced accordingly. We should also point out that for a double-couple of this size and orientation the group delay at the source is quite small. As long as $F < 1$, the double-couple has almost no affect on the seismogram except to scale its amplitude. The same is true for larger F if we are on a positive lobe of the radiation pattern. This is illustrated in Figure 19 where the theoretical seismogram for PILEDRIVER at TUC from Figure 5 is compared to similar seismograms with the source including a strike-slip double-couple component.

The double-couple components for the seismograms of Figure 19 are computed using the tectonic release model of Archambeau (1972). If the tectonic stress release has the sense of pure strike-slip faulting, the F factor is related to the parameters of the model by

$$F = \frac{15}{46} \frac{\sigma_{xy} R_o^3}{\mu_s \Psi_\infty}$$

where σ_{xy} is the horizontal stress drop and R_o is the radius of the spherical volume in which this (average) stress drop occurs. For example, if the PILEDRIVER yield is 56 KT and $\mu_s = 206$ kbar, several values of R_o , σ_{xy} and Ψ_∞ at 0.02 KT that lead to $F = 3.2$ are given below

<u>$\Psi_\infty 0.02$ (m³)</u>	<u>R_o (m)</u>	<u>σ_{xy} (bars)</u>
4	609	100
4	484	200
2	300	419
8	609	200

Interpretation of F in terms of a plane strike-slip dislocation can also be made. The moment for the Archambeau source is (Minster and Suteau, 1977)

$$M_o = \frac{60}{23} \pi \sigma_{xy} R_o^3 ,$$

while for a dislocation source it is

$$M_o = \mu_s S D$$

where S is the fault area and D is the average dislocation. Therefore,

$$F = \frac{S D}{8\pi \Psi_\infty}$$

and a table like that given above for the Archambeau source is easily constructed.

In Table 8 are given the corrected values of Ψ_∞ computed by dividing the mean values of Table 4 by the mean double-couple enhancement from Table 7. These corrections are rather crude, but do indicate the trend of the correction and, roughly, its magnitude. For Yucca Flat and Pahute Mesa the corrected solutions are quite satisfactory and might be preferred to those in Table 4. For PILEDRIVER the new Ψ_∞ values in Table 8 are quite small and are difficult to justify when compared to theoretical and empirical data (see Table 6).

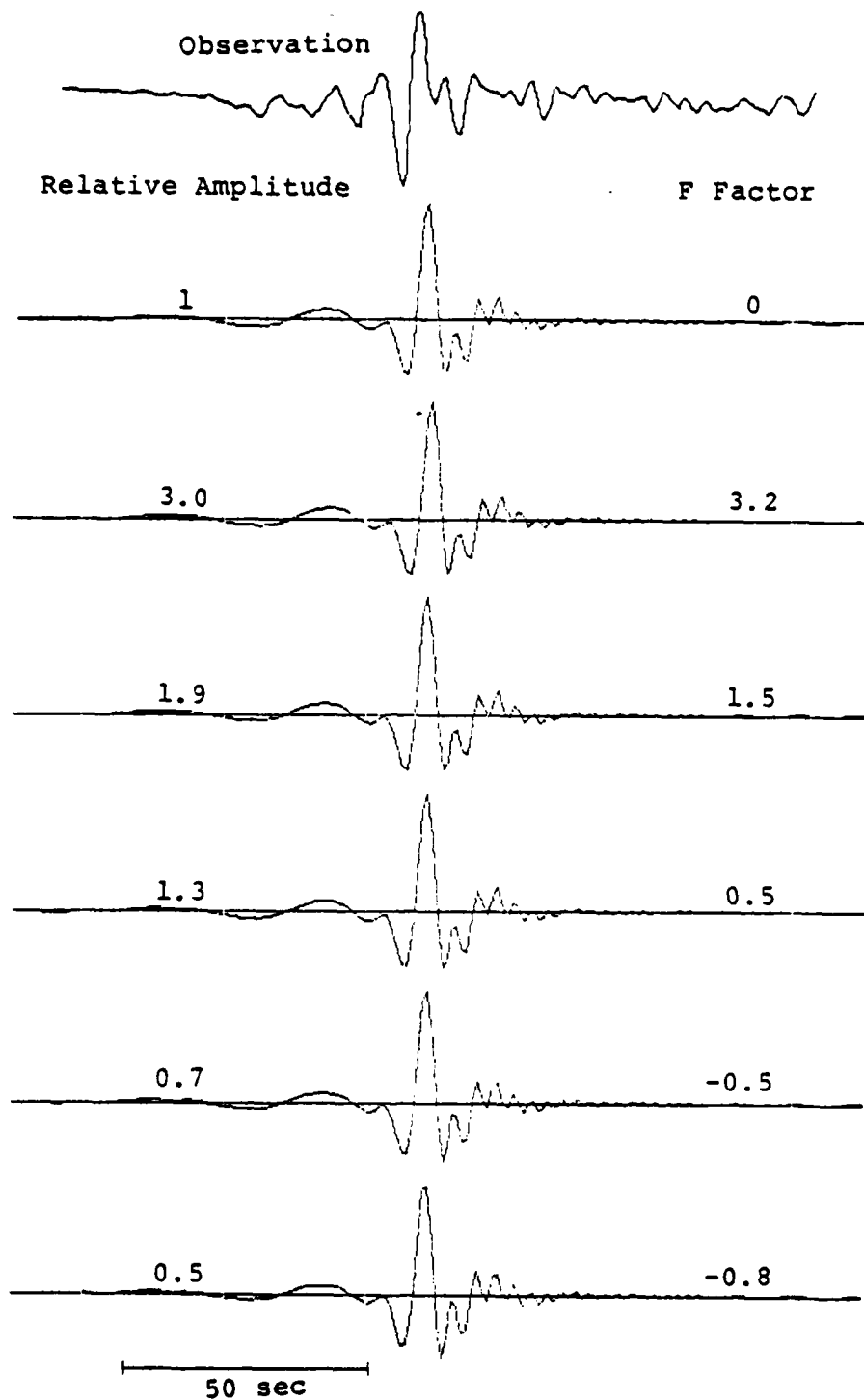


Figure 19. Theoretical seismograms for PILEDRIVER at TUC are shown for a composite source including the explosion plus a strike-slip double-couple. The azimuth is 157° clockwise from the strike and the relative size of the double-couple is indicated by the F factor with a negative F signifying that the station is on the negative lobe.

TABLE 8

INFERRED Ψ_∞ VALUES CORRECTED BY THE DOUBLE-COUPLE
FACTORS FROM TABLE 7

<u>Events</u>	<u>ALQ Ψ_∞</u>	<u>TUC Ψ_∞</u>	<u>$\frac{\Psi_\infty(\text{TUC})}{\Psi_\infty(\text{ALQ})}$</u>
Yucca Flat	7.6	9.7	1.28
Pahute Mesa	4.1	6.1	1.49
PILEDRIVER	1.1	2.1	1.88

VI. CORRECTION FOR THE EFFECT OF SURFACE SPALLATION

6.1 Introduction

Underground nuclear explosions almost always cause spallation near the free surface (e.g., Eisler and Chilton, 1964). When the spalled material falls back to the surface (spall closure), some impulse is delivered and a large signal associated with spall closure can often be observed on near-field recordings (e.g., Eisler, *et al.*, 1966; Toman, *et al.*, 1973). These data can be used to estimate the dynamics of the spall zone and its extent (e.g., Chilton, *et al.*, 1966; Viecelli, 1973; Sobel, 1978). Viecelli (1973) suggested that the spall closure makes a large contribution to the recorded Rayleigh waves in the far-field. If this were true, it would strongly compromise the results of our analysis in previous sections.

In this section we first summarize the estimates for the extent of spall given by Viecelli and by Sobel (1978). Following Viecelli, we use these estimates to bound the amplitude of the impulse applied by spall closure. Using some theoretical results given by Harkrider, *et al.*, (1974), we then compute the Rayleigh waves due to spall.

If large amounts of energy are trapped in the spall zone, we should also account for the loss of this energy from the calculation of the explosion produced Rayleigh waves. We approximate this by deleting from the Rayleigh wave calculation all or a portion of the upward traveling energy from the explosion. The Rayleigh waves generated by the spall closure are then superimposed on this truncated source.

In summary, to account for the effect of surface spallation it is necessary to subtract some portion of the explosion energy and then to add the energy from the spall closure. In view of the approximations involved, this cannot

be done with much certainty. However, experiments with plausible values for the governing parameters allow estimation of some bounds on the spall contribution.

6.2 Estimation of the Impulse due to Spall Closure

Using data from surface accelerometers, some estimates can be made for the extent of the spall region (Eisler and Chilton, 1964; Viecelli, 1973; Sobel, 1978). Viecelli (1973) studied the data for six explosions, two in Rainier Mesa tuff and four in Pahute Mesa tuff and rhyolite. Assuming a density of 2 gm/cm^3 , he estimated the mass of the upthrown material to be

$$\langle M \rangle \approx 1.6 \times 10^{12} W \text{ grams} , \quad (10)$$

where W is the yield in kilotons. Sobel (1978) carried out a similar study, looking at the near-field data from some twenty-six events in a variety of materials. Using her derived relations for the dimensions of the spall zone and $\rho = 2 \text{ gm/cm}^3$, the estimate for the mass is

$$\langle M \rangle \approx 10 \times 10^{12} W^{.97} \text{ grams} . \quad (11)$$

The factor of six difference between the two estimates is mainly due to different methods for estimating the maximum extent of the spall zone.

Assuming a conical displacement profile, Viecelli estimated the total downward impulse due to the spall plate falling back to be

$$\langle I \rangle \approx \frac{\langle M \rangle}{3} (2g h_0)^{1/2} , \quad (12)$$

where g is the gravitational acceleration and h_o is the maximum height of spall. Using Viecelli's estimates for the spall dimensions,

$$\langle I \rangle \approx 4.6 \times 10^{14} W \text{ dyne-sec}; \quad (13)$$

while the dimensions found by Sobel lead to

$$\langle I \rangle \approx 8.6 \times 10^{14} W^{1.15} \text{ dyne-sec} . \quad (14)$$

At 100 KT these estimates differ by a factor of 3.7.

The temporal and spatial distribution of the spall closure is quite small compared to the periods and wavelengths of primary interest and it seems reasonable to represent this source as an impulse load at the surface. The question is then, how good are the estimates in (13) and (14) for the amplitude of this impulse?

The mass was computed by assuming that the volume of the spall can be approximated by a circular disk of uniform thickness. Then the impulse is proportional to $\rho r_s^2 D h_o^{1/2}$ where ρ is density, D is the thickness of the spall plate and r_s is its radius. The spall thickness is about 100m for 100KT and is proportional to $W^{1/3}$. At depths this shallow the average density is probably closer to 1.7 gm/cm^3 than to 2 gm/cm^3 , the value used to compute (10) and (11). Using $\rho = 1.7$, our impulse estimates are reduced by 15 percent.

The h_o is determined from surface measurements and is attributed entirely to separation at the single depth D . Since the total surface displacement includes contributions from spallation at many depths (Eisler, et al., 1966) the latter assumption is likely to lead to an overestimate of the spall impulse, even if the estimates for r_s and D are accurate.

If we assume N spall plates of thickness D_j separated by openings h_j , $j = 1, \dots, N$, then the total impulse is proportional to

$$\sum_{j=1}^N D_j \left(\sum_{i=1}^j h_i \right)^{1/2}. \quad (15)$$

Given that $\sum_{j=1}^N D_j = D$ and $\sum_{j=1}^N h_j = h_o$, it is easily shown that this factor must be less than or equal to $Dh_o^{1/2}$, its $N=1$ value.

The conclusion that the impulse in (14) is an overestimate was also drawn by Sobel (1978) after studying subsurface accelerometer records. She found the spall energy leaving the source region to be much smaller than expected from her estimates of the extent of spall and attributed the discrepancy to the pressure of multiple spall openings.

Another question to be addressed is the time lag between the explosion and the spall closure. It is easily shown that this time lag T_L is

$$T_L = T_s + 2 \sqrt{\frac{2g h_o}{g}}, \quad (16)$$

where T_s is the time when spall parting occurs. For explosions in tuff at a scaled depth of $122 W^{1/3}$, $T_s \approx .06 W^{1/3}$. At 100 KT this is 0.28 seconds. The second term in (16) is the time the spall remains open. If there is only one spall opening, Sobel's results give $.52 W^{1.75}$ for this time (1.2 seconds at 100 KT) while Viecelli finds a yield independent value of 1.75 seconds. Therefore, for yields of 50 to 200 KT the total T_L is 1.3 to 2.0 seconds, assuming a single spall parting. For multiple spall openings the second term in (16) is reduced the same way the impulse is reduced by multiple spall partings. Since this term dominates and multiple spall partings do occur, a lag of about 1 second is thought to be most appropriate.

6.3 Calculation of Rayleigh Waves from the Spall Closure Impulse

We assume that spall closure can be represented as an applied normal force at the surface of a multilayered halfspace. Harkrider, et al., (1974) gives the expressions for the Rayleigh waves due to loading of this kind. The vertical (positive downward) displacement is

$$\hat{w}_s(r, \omega) = -i\pi \hat{A}_R \hat{P}(\omega) H_o^{(2)}\left(\frac{\omega r}{c}\right), \quad (17)$$

where we have introduced the notation

$$\hat{A}_R = -i \frac{(GN - LH)}{\left(\frac{\partial F_R}{\partial k}\right)} \quad (18)$$

for the amplitude excitation following Harkrider (1964). The source term is

$$\hat{P}(\omega) = \int_0^{\infty} P_o(r, \omega) J_o\left(\frac{\omega r}{c}\right) r dr, \quad (19)$$

where $P_o(r, \omega)$ is an azimuthally symmetric Fourier time-transformed normal stress distributed on the surface. If the spatial extent and time duration of the surface load are small compared to wavelengths and periods of interest, the total impulse is

$$\langle I \rangle = 2\pi \hat{P}. \quad (20)$$

Using separate models for the local source region and the remainder of the path, the expression for the spall induced Rayleigh waves that is analogous to Equation (1) for an explosion is

$$\hat{w}_s(r, \omega) = -i\pi P(\omega) A_{R_1} T(\omega) H_0^{(2)}\left(\frac{\omega r}{c_2}\right) e^{-\gamma r} \cdot \left(\frac{r}{a_e \sin \Delta}\right)^{1/2} \quad (21)$$

where terms for the attenuation and sphericity correction have also been introduced.

Comparing (1) and (21) we see that a spherically symmetric explosion and a spall closure source give identical Rayleigh waves when

$$4\mu_s \hat{\Psi} \frac{K_{s_1}}{c_1} = i \hat{P} \quad (22)$$

For explosions in Yucca Flat tuff our models give $|K_{s_1}/c_1|$ to be about 0.39 sec/km at 10 seconds. Then the spectral amplitudes for the two sources are the same when

$$2.45 \times 10^{13} \hat{\Psi}_\infty^{0.02} = \hat{P} \quad (23)$$

where $\hat{\Psi}_\infty^{0.02}$ is the zero frequency value of $\hat{\Psi}$ in m^3 scaled to 0.02 KT. If the scaled $\hat{\Psi}_\infty$ is about 10, a reasonable value for Yucca Flat tuff (Table 4), the impulse calculated by Viecelli, Equation (13), gives Rayleigh waves about 30 percent as large as those from the explosion. For yields around 100 KT Sobel's estimate, Equation (14), gives Rayleigh waves that are the same size as those from the explosion. We have already said that the impulse values in Equations (13) and (14) appear to be overestimated. However, they are large enough that we must explore their potential influence more carefully.

In Figure 20 we show the effect of adding Rayleigh waves from the spall closure impulse to the Rayleigh waves from the spherically symmetric source for a typical Yucca Flat event. The top two records are the TAN observations and synthetic seismograms from Figure 5. We then show the Rayleigh waves from the spall closure computed using Equation (21). The $P(\omega)$ was assumed to be an impulse source, Equation (20), so the amplitude of the signal is directly proportional to the size of the impulse. The last three records show the effect of summing the explosion and spall produced Rayleigh waves. There are two parameters for the summation, the lag time T_L and the ratio of impulse and explosion sources, P/Ψ_∞ , which is motivated by (23). In this context $\Psi_\infty = \Psi_\infty^{0.02} W/0.02$.

The summed seismograms in Figure 20 were done for two lag times and two P/Ψ_∞ ratios. For an event like TAN, a one second T_L seems more appropriate, though somewhat larger values are possible. The P/Ψ_∞ ratios can be interpreted in terms of the impulse and compared to the estimates of Viecelli and Sobel in Equations (13) and (14). From (20) we have

$$\langle I \rangle = 2\pi n (6.2 \times 10^{12}) \Psi_\infty^{0.02} W , \quad (24)$$

where n is 1 or 2 for the seismograms in Figure 20. Then if $\Psi_\infty^{0.02} = 11.8 \text{ m}^3$, the impulse is 1.0 or 2.0 times the impulse estimate of Viecelli. For $n = 2$, the impulse is 1.7 to 2.1 times smaller than Sobel's estimate at 50 to 200 KT. It is probably not reasonable to expect an impulse much larger than this.

The first thing we notice about the composite records in Figure 20 is that the waveform is not greatly changed by the addition of the spall closure contribution. In fact, at ALQ the change is hardly perceptible. At TUC the second trough is reduced and the agreement with the observed record is actually enhanced. The relative amplitudes of the phase

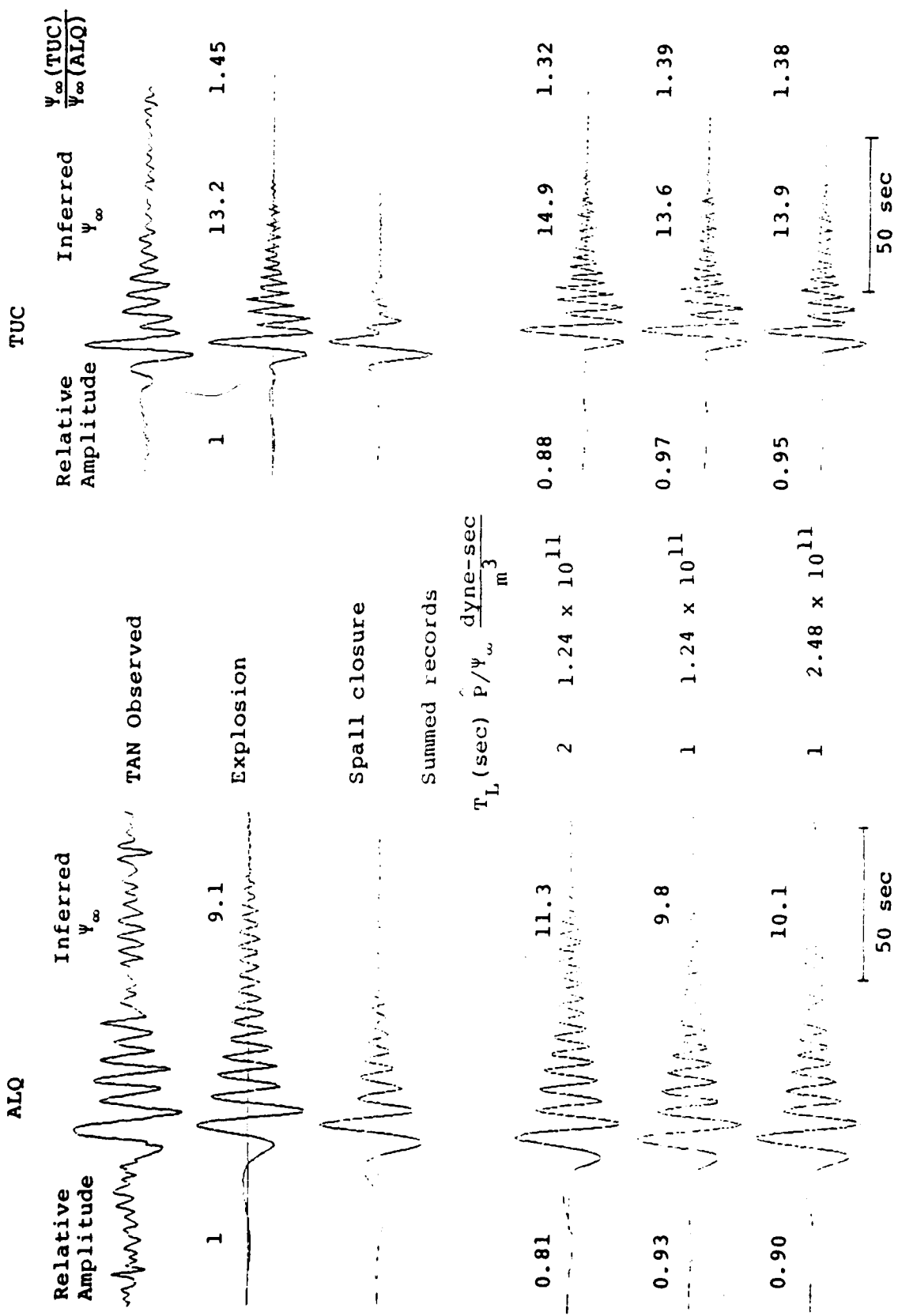


Figure 20. The effect of the spall closure impulse on the Rayleigh waves for Yucca Flat explosions is shown for two lag times and two spall impulse amplitudes.

corresponding to the maximum peak-to-peak excursion on the observation is also indicated on the plots. The effect is a little greater at TUC than at ALQ, but is less than 20 percent for every case.

Since the effect of the spall impulse contribution is to reduce the Rayleigh wave amplitude, we would account for this effect by increasing our estimate for the Ψ_∞ due to the explosion itself. The increase is, of course, by the inverse of the relative amplitudes. The new inferred values are shown on Figure 20. (The spall closure impulse is also increased by the same amount since P/Ψ_∞ is fixed). These values are not specifically for TAN but are based on the mean Yucca Flat Ψ_∞ given in Table 4. The effect on the TUC/ALQ ratio is also shown on the plot. The addition of a spall contribution causes the discrepancy between the ALQ and TUC estimates to be reduced a little.

The spall contribution might be expected to be quite variable and could account for some of the scatter in our Ψ_∞ estimates for Yucca Flat events, though it would be surprising if it introduced scatter much bigger than 10 to 20 percent. Some evidence for the consistency of this contribution is the remarkable similarity in the waveforms for different events (Figure 1).

What about the effect of spall closure on the signals from events in other materials, the Pahute Mesa tuffs and rhyolites and the PILEDRIVER granite? We have no reason to suppose the dimensions of the spall zone are dependent on the source material. Viecelli's estimates are actually based predominantly on observations of Pahute Mesa events. Sobel looked at events in many materials but no systematic dependence on source material is discernible. Since the density of the near surface materials is likely to be pretty much the same at all these areas, we can only conclude that the impulse estimates in (13) and (14) are valid for all three areas.

The major factor that distinguishes Yucca Flat from the other testing areas in regard to the contribution from spall closure is the substantially smaller value of $\mu_s \Psi_\infty$ for the Yucca Flat events. In view of (22), this means that a larger impulse is required to have the ratio of the spall closure to explosion Rayleigh waves be the same at Pahute Mesa and PILEDRIVER as it is at Yucca Flat. The pertinent numbers are given in Table 9. We see that the impulse must be about twice as big for Pahute Mesa and PILEDRIVER events to have the same relative contribution as at Yucca Flat. From the Yucca Flat example in Figure 20, one would conclude that the potential contribution of the spall closure can be neglected for the other two areas. However, before closing this subject, we need to look at the effect of deleting the portion of the explosion energy that is absorbed in the spallation process.

6.4 Modification of the Explosion Source to Account for Energy Lost to Spallation

It is inconsistent to add a downward impulse source to represent the spall closure while continuing to model the explosion as a spherically symmetric point source in a layered elastic halfspace. The energy for the spallation comes from the waves propagated upward from the source. Thus, if a large amount of spallation occurs, we expect a substantial reduction in the body wave phase pP from what is predicted by elastic theory.

Our theoretical formulation for computing Rayleigh waves can be modified to allow total or partial suppression of the source radiation emitted upward or downward from the source. For a spherically symmetric source this is done by replacing the depth-dependent excitation factor K_{s1} in Equation (11) by

TABLE 9
IMPULSE FOR A FIXED RATIO OF SPALL CLOSURE
TO EXPLOSION RAYLEIGH WAVES

Test Area	Mean* $\Psi_{\infty}^{0.02}$	μ_s (kbar)	K_{s1}/c_1 (10 sec)	$4\mu_s \Psi_{\infty}^{0.02} K_{s1}/c_1$	Normalized Impulse
			(sec/km)		
Yucca Flat	11.2	31.4	0.39	2.74×10^{14} W	1
Pahute Mesa	9.9	96.6	0.35	6.02×10^{14} W	2.2
PILEDRIVER	5.1	206	0.24	5.04×10^{14} W	1.8

*The mean $\Psi_{\infty}^{0.02}$ is the average of the mean values for ALQ and TUC from Table 4.

$$\frac{(2 - |\Gamma|)}{2} K_{s_1} - i\Gamma M_{s_1} , \quad (25)$$

$$\frac{4\mu_s r_\alpha}{\dot{w}_o/c_1}$$

where

$$K_{s_1} = \frac{1}{2\mu_s} \frac{\sigma_s(h)}{\dot{w}_o/c_1} - \frac{\dot{u}_s(h)}{\dot{w}_o} ,$$

$$M_{s_1} = \left(\rho_s c_1^2 - 2\mu_s \right) \frac{\dot{w}_s(h)}{\dot{w}_o} - \frac{\tau_s(h)}{\dot{w}_o/c_1} ,$$

$$r_\alpha = \left(\frac{c_1^2}{\alpha^2} - 1 \right)^{1/2} ,$$

$\Gamma = 1$: All upgoing waves suppressed,

$\Gamma = 0$: Total solution

$\Gamma = -1$: All downgoing waves suppressed.

The stress and displacement eigenfunctions in the definitions of K_{s_1} , M_{s_1} are defined by Harkrider (1964, 1970). The Γ can take any value in the range $[-1, 1]$, and represents the proportion of up or downgoing waves suppressed.

In the formulation of Equation (25) Γ may be constant or it may be frequency dependent. In the applications here, we will assume a constant Γ , mainly because we have no firm basis for doing otherwise. As far as deleting the energy lost to spallation is concerned, it might be more reasonable to suppose that this occurs mostly at the high frequencies and the low frequencies are much less affected. More theoretical work is required to develop this line of reasoning much farther.

In a previous report (Bache, Goupillaud and Mason, 1977), we studied the effect of suppressing various proportions of the upgoing waves on the Rayleigh waves at 3,000 km. The two cases examined were like the Yucca Flat and PILEDRIVER events studied here. For the Yucca Flat-like event we found that suppression of the upgoing wave tends to increase M_s compared to the total source because the upgoing and downgoing portions of the wave field generate Rayleigh waves that destructively interfere. On the other hand, for the PILEDRIVER-like event, suppression of the upgoing waves substantially reduced M_s because the Rayleigh waves from the two parts of the source are in phase and that from the upgoing waves is considerably larger. These conclusions were based on the well dispersed 20 second waves on the teleseismic records. However, similar results are obtained for the Airy phase of interest at ALQ and TUC.

The different contributions of the upgoing and downgoing waves for events in granite compared to those in Yucca Flat tuff can be, in large part, attributed to the importance of S waves for Rayleigh wave generation. For spherically symmetric explosions in granite the only large source of S waves is the pS conversion at the free surface which is deleted when the upgoing waves are suppressed. However, there is a strong impedance contrast below the source for Yucca Flat events (Figure 6), which continues to generate S waves in the absence of the pS conversion at the free surface.

In Figure 21 we show the following seismograms for our representative Yucca Flat event (TAN) at ALQ and TUC:

- A. The observation.
- B. The synthetic for the spherically symmetric explosion (Figures 5 and 20).
- C. The synthetic for the source with all upgoing waves suppressed.

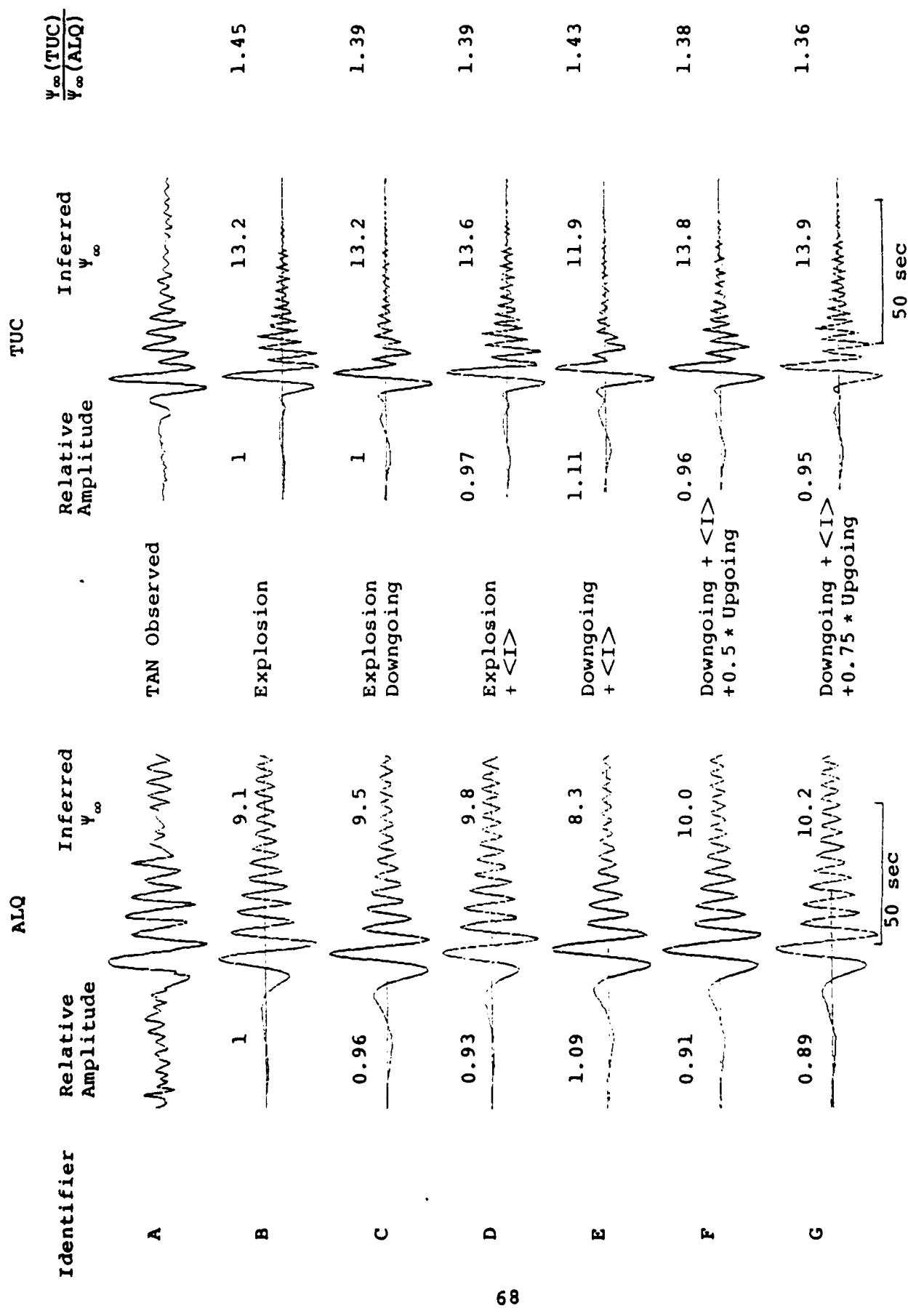


Figure 21. Synthetic seismograms for a variety of source representations for a Yucca Flat event. For the spall impulse $T_L = 1$.

- D. A composite synthetic including the total source plus the spall contribution with $\hat{P}/\Psi_\infty = 1.24 \times 10^{11}$ and $T_L = 1$ second (Figure 20).
- E. A composite synthetic with only the downgoing waves from the explosion (C) and the same spall contribution as in D.
- F. A composite synthetic with half the upgoing waves suppressed and the same spall impulse as D.
- G. A composite synthetic with 25 percent of the upgoing waves suppressed and the same spall impulse as D.

A key feature of these synthetic seismograms is that the amplitudes vary within about ± 10 percent of that for the spherically symmetric point source model. Thus, our assumptions about the spalling and degradation of the upgoing waves are not too important. For each seismogram in Figure 21, we also list the inverse of the relative amplitude times the mean Yucca Flat Ψ_∞ from Table 4. This shows the amount by which the inferred Ψ_∞ values are corrected by the effects represented in each synthetic record.

The span of reasonable models is believed to be represented by seismograms B, C, F and G, though the impulse contribution may be overestimated. (For $\Psi_\infty = 11.8$, the impulse has the amplitude estimated by Viecelli, Equation (13)). These indicate that the effect of spall-related phenomena is likely to increase the inferred Ψ_∞ by a small amount, perhaps 5 to 10 percent. The discrepancy between the ALQ and TUC Ψ_∞ estimates is also reduced slightly.

Some evidence for the preferred model can be deduced from the comparison of theoretical and observed waveforms. The explosion itself, Case A, provides a good fit at both stations and addition of the spall closure impulse, Case D, seems to improve it. However, the fit is substantially degraded by deleting the upgoing waves. Therefore, the best

fit to the waveform is by the seismograms in which little or none of the upgoing waves are deleted, Cases D and G. Taking all factors into consideration, we prefer the model for Case G.

For PILEDRIVER, or other explosions in granite, the story is quite different. Our assumptions about spallation, and especially the degradation of the upgoing waves, have a strong influence on the amplitude of the synthetic seismograms. Synthetic seismograms for granite are shown in Figure 22. The seismograms are analogous to those in Figure 21 except that the amplitude of the spall closure impulse has been adjusted to be about the same for Cases D to G while the inferred Ψ_∞ varies over a wide range. The impulse values for the mean of the ALQ and TUC inferred $\Psi_\infty^{.02}$ are as follows:

Case	\hat{P}/Ψ_∞ (dyne-sec)	Inferred	$\langle I \rangle$ (dyne-sec)
	$\frac{m^3}{m}$	$\Psi_\infty^{.02}$	
D	4.1×10^{11}	5.3	6.8×10^{14} W
E	1.24×10^{11}	19.6	7.6×10^{14} W
F	2.1×10^{11}	8.3	5.3×10^{14} W
G	2.1×10^{11}	6.4	4.1×10^{14} W

Therefore, the impulse added to the source is about the same size as for the Yucca Flat event in Figure 21 and is comparable to the value (4.6×10^{14} W) found by Viecelli.

The major factor controlling the PILEDRIVER seismograms is the proportion of upgoing waves deleted. The amplitude of the seismogram for the total source is nearly four times as large as that from the downgoing waves alone (compare B and C). The spall closure impulse, as expected, has a relatively small effect. Therefore, the amount of upgoing energy that is lost to spall or scattered is of great importance for determining the granite source. The waveform fit does not help

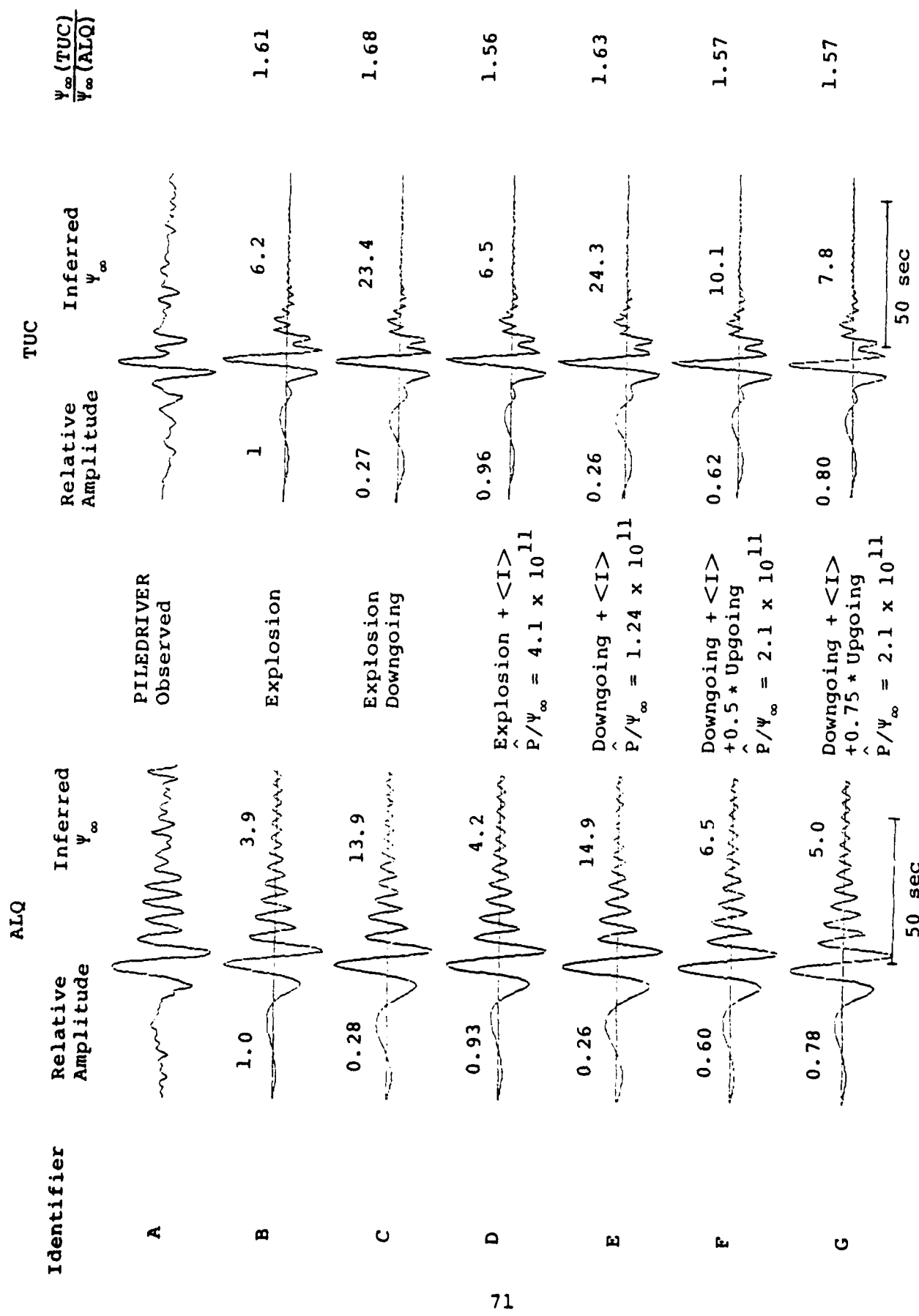


Figure 22. Synthetic seismograms for a variety of source representations for PILEDRIVER. For the spall impulse $T_L = 1$.

us to choose between the alternatives. The fit to the ALQ observations is equally good for all cases. At TUC the fit is poorer than at ALQ and is not much better for one case than for another.

The analysis of PILEDRIVER is further complicated by the presence of a large double-couple component in the source for surface waves. As we pointed out in Section V, the double-couple solution of Toksöz and Khrer (1972) predicts double-couple radiation that dominates the Rayleigh wave (Table 7). The waveform from the double-couple is nearly the same as that from the explosion alone (Figure 19). We must take all these factors into account when developing our final solution for PILEDRIVER.

The events at Pahute Mesa are more nearly like PILEDRIVER than the Yucca Flat events as far as the effect of spallation is concerned. The pertinent synthetic seismograms are shown in Figure 23 in the same format as used in Figure 21 and 22, except that Cases C and E are not shown. The amplitude of the spall closure impulse for these seismograms is as follows:

<u>Case</u>	$\hat{P}/\psi_\infty \left(\frac{\text{dyne-sec}}{\text{m}^3} \right)$	<u>Inferred</u> ψ_∞	<u>$\langle I \rangle$ (dyne-sec)</u>
D	1.86×10^{11}	9.5	5.6×10^{14} W
F	2.48×10^{11}	11.1	8.6×10^{14} W
G	2.48×10^{11}	13.0	10.1×10^{14} W

This impulse ranges from 1.2 to 2.2 times as large as that found by Viecelli (1973) for Pahute Mesa events.

As with PILEDRIVER, suppression of a portion of the upgoing waves has a strong effect on the amplitude of the explosion source required to match the observations. We also note that the spallation effects seem to increase the difference between the ALQ and TUC estimates. The agreement of observed and theoretical seismograms is quite good for both stations and seems to be independent of our assumptions about the source.

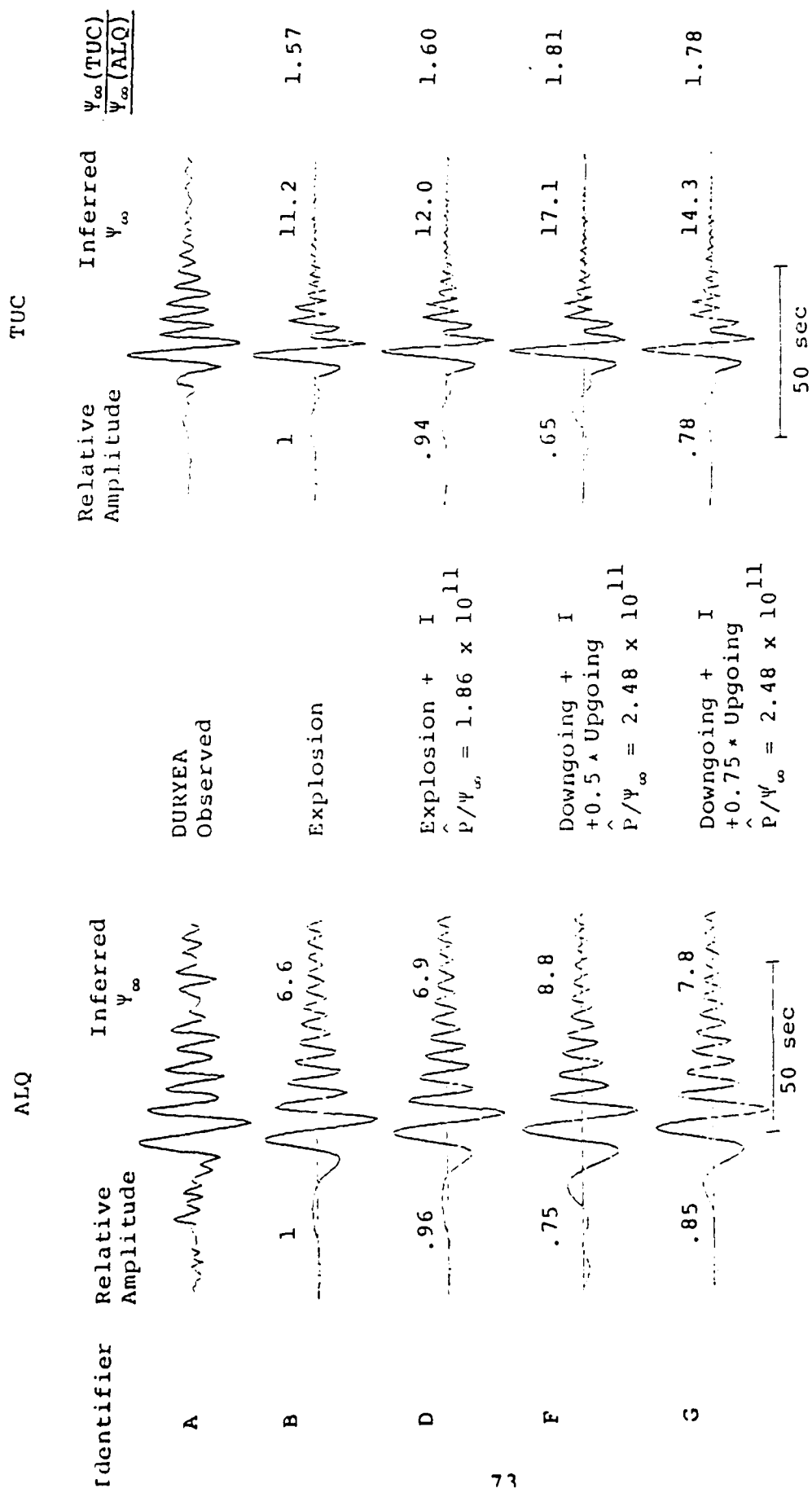


Figure 23. Synthetic seismograms for a variety of source representations for a Pahute Mesa event.

An important conclusion of this analysis of the spall effects is that it is not the spall closure impulse that is important, but the possible loss of energy from the upgoing waves. At this time we can only speculate about this and outline its potential influence. Independent studies are needed to develop a better understanding of this phenomenon. A great deal could be learned from two-dimensional finite difference calculations in which spallation is allowed to occur.

6.5 Simultaneous Correction for the Spall Impulse and Double-Couple Contributions to the Source

In Section V we discussed the double-couple enhancement of the source according to the results of Toksöz and Kehrer (1972). For PILEDRIVER the double-couple source dominates the Rayleigh wave, while it plays a relatively small role for most of the other events (Table 7). In simultaneously including all the effects we have discussed, we must decide what to do with the upgoing waves generated by the double-couple source. If this source is spatially and temporally contiguous with the explosion, then both components of the source should be treated the same. If not, we may want to suppress only the upgoing waves from the explosion and leave the double-couple unchanged. Let us examine the effect of these alternatives.

In Figure 24 we show the PILEDRIVER synthetic seismogram at TUC with a double-couple of strength $F = 3.2$. The same record appeared in Figure 19. We then suppress 25 percent and 50 percent of the upgoing waves from the total source.* The effect is quite strong with the amplitude reduction being proportional to the fraction of upgoing waves suppressed.

*The formulation of the theory for suppressing the upgoing waves is due to D. G. Harkrider.

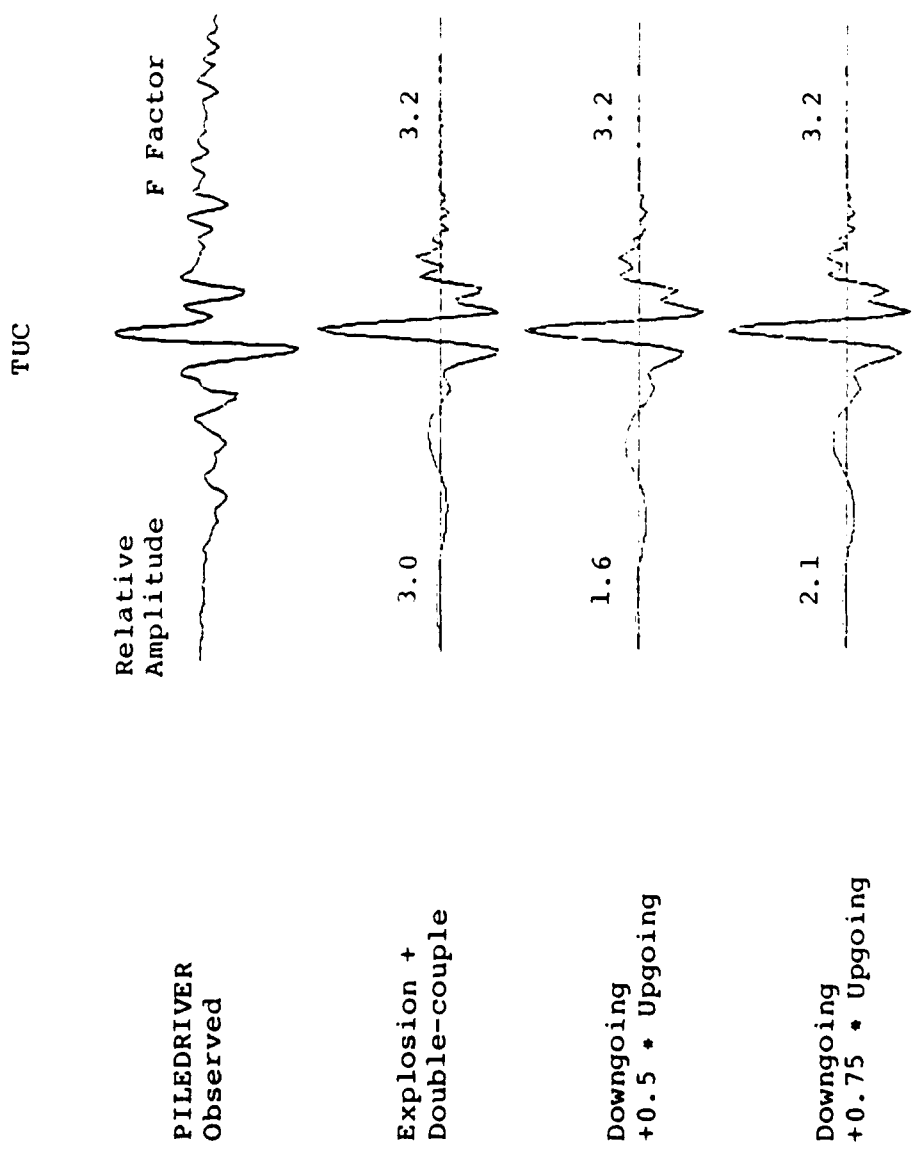


Figure 24. Theoretical seismograms at TUC for PILEDRIVER represented by a source including explosion and double-couple components. A portion of the upgoing waves is suppressed as indicated.

The match to the observed waveform at TUC is not nearly as good for PILEDRIVER as it is for the Pahute Mesa and Yucca Flat events, no matter what we assume about the source. There seems to be something about this event that is not accounted for in our models.

If we do not suppress any of the upgoing wave energy from the double-couple, simultaneous correction for double-couple and spallation effects is done by a simple superposition. The double-couple correction factors used in Section V are applied to the composite source solutions of Figures 21 to 23. The results are given in Table 10.

Our final results are summarized in Table 10. We first list the mean source amplitude obtained when assuming the reduced displacement potential represents the entire source. The mean double-couple corrections deduced in Section V are then listed as are our preferred solutions for the spall-corrected source level. The latter are from the composite source with 25 percent of the upgoing waves suppressed in Figures 21 to 23. The new corrected source level is then obtained by dividing the spall-corrected source by the double-couple correction.

For PILEDRIVER we give two solutions with the first obtained as outlined above. If we suppress the upgoing waves from the double-couple in the same proportion as from the explosion, the Rayleigh waves are reduced as shown in Figure 24. The double-couple correction is reduced accordingly; that is, by two-thirds for suppression of 25 percent of the upgoing waves.

For the Yucca Flat events, the solutions are quite satisfactory. For Pahute Mesa events, the main issue is the extent of suppression of the upgoing waves by scattering and spallation. More theoretical work, particularly in the two-dimensional modeling of explosions, is required to develop

TABLE 10
SIMULTANEOUS CORRECTION FOR THE EFFECT OF SPALLATION
AND A SUPERIMPOSED DOUBLE-COUPLE

	<u>ALQ</u>	<u>TUC</u>	<u>Ψ_∞ (TUC)</u>
			<u>Ψ_∞ (ALQ)</u>
<u>Yucca Flat</u>			
Explosion source (Table 4)	9.1	13.2	1.50
Double-couple correction (Section V)	1.19	1.36	-
Spall corrected source (Figure 21)*	10.2	13.9	1.36
New corrected source	8.6	10.2	1.19
<u>Pahute Mesa</u>			
Explosion source (Table 4)	6.6	11.2	1.57
Double-couple correction (Section V)	1.62	1.84	-
Spall corrected source (Figure 23)*	7.8	14.3	1.70 [†]
New corrected source	4.8	7.8	1.50
<u>PILEDRIVER</u>			
Explosion source (Table 4)	3.9	6.2	1.59
Double-couple correction (Section V)	3.55	3.00	-
Spall corrected source (Figure 22)*	5.0	7.8	1.56
New corrected source	1.4	2.6	1.85
Modified double-couple source (Figure 23)*	2.1	3.8	1.81

* Based on suppression of 25 percent of the upgoing waves.

† The mean ratio after correcting each event individually.

a clearer understanding of this effect. For PILEDRIVER, there are several aspects that remain puzzling. The source levels are quite small, perhaps too small to be consistent with the evidence from other types of data (Table 6). The discrepancy between the ALQ and TUC estimates is very large, especially when compared to that for the other events. Finally, we have the relatively poor match between the synthetic and observed records at TUC. Considering all this, we have much less confidence in our source estimate for PILEDRIVER.

The difficulty with the PILEDRIVER source estimate is that it is strongly influenced by two poorly understood effects. The explosion source level is small because most of the Rayleigh wave is from the double-couple if the Toksöz and Kehrer (1972) solution is used. But suppression of the upgoing waves has an equally strong effect, increasing the inferred source level. At this time, we are unable to resolve these conflicting effects, but only point them out and indicate their importance.

VII. EXAMINATION OF THE DIFFERENCES BETWEEN THE ALQ AND TUC SOURCE ESTIMATES

If a spherically symmetric point source is assumed, the source level inferred from the TUC observations is about 1.5 times larger than that inferred from the ALQ observations (Table 4). This difference is quite consistent; averaging all 22 events in the population of Table 4, the ratio is 1.52 with a standard deviation that is 25 percent of the mean. The question is, why should the source appear larger when viewed from TUC than when viewed from ALQ? One possible explanation is that there is a true asymmetry at the source that causes Rayleigh waves to be more strongly excited toward TUC. In the last two sections we saw that correcting for the double-couple and spall closure contributions does remove much of the difference for Yucca Flat. However, this explanation does not seem to work for PILEDRIVER and Pahute Mesa.

A likely cause for differences in the Ψ_∞ estimates at the two stations is that our plane-layered models are unable to represent the laterally varying non-planar earth with the same accuracy for both paths. Lateral heterogeneities can certainly cause amplitude variations by focusing or defocusing the surface waves at a particular site. Von Seggern, et al., (1975) discuss focusing due to lateral variations in Rayleigh wave phase velocity and show that effects of the size seen here can occur. Focusing that would account for the asymmetry in the inferred source amplitude must act to increase the observed amplitudes at TUC and/or decrease those at ALQ.

One lateral inhomogeneity we know about is the crustal thickening along the NTS-ALQ path. It is plausible to suppose that this inhomogeneity causes the surface waves at ALQ to be smaller than predicted by our plane-layered model. Such an error would cause us to underestimate the Ψ_∞ from the ALQ data, leading to the kind of asymmetry we see.

For our plane-layered models there are four main factors controlling the amplitude of the synthetic seismograms that should be examined more closely. There are the dispersion, the choice of the structure in the source region, the transmission between the source and path structures and the Q models for the two paths.

The average dispersion data is matched about as well for the NTS-TUC path as for the NTS-ALQ path (Figures 3 and 4), though the dispersion data itself is better determined for the NTS-ALQ path (Figure 2). The TUC seismograms are dominated by a strong Airy phase at about 8 seconds, which does make this station more difficult to analyze. We can see in the comparison of synthetic and observed seismograms in Figure 5 that subtle interference effects control the peak amplitude at TUC to a greater degree than at ALQ. In fact, the comparison suggests that our synthetic seismograms probably underestimate the Airy phase amplitude at TUC. However, while this error does contribute to the Ψ_∞ asymmetry we are discussing, it is probably not much larger than 10 percent.

In computing the theoretical seismograms, we have assumed that the amplitude excitation is the same for both paths. Calculations of theoretical seismograms for the two paths differ only in the dispersion and the transmission coefficient, $T(\omega)$. The source region models were based on the structure for the NTS-TUC path which lies entirely in the Basin and Range Province, and this is certainly more reasonable if we want to use the same source region model for both paths. One could argue that the NTS-ALQ synthetics are more accurately computed with source region models based on the NTS-ALQ crustal structure. However, if we do so, we increase the ALQ Ψ_∞ estimates by only about 5 percent. This is in the right direction, but is too small to have much significance.

The transmission coefficient, $T(\omega)$, is not a well defined parameter. It is meant to account for a gradual transition between the source region model and the average model for the travel path. There are probably many gradual transitions that are averaged in our procedure. As we discussed in connection with Figure 7, the $T(\omega)$ are near unity for periods of primary interest and play no significant role in the calculation except at short periods where they do help shape the waveform. This is, of course, because our source and path structures differ greatly only near the surface.

Perhaps the least understood feature of the calculations is the appropriate $\gamma(\omega)$ or Q model to be used for each path. The attenuation models we used (Table 3) are related in that the Q- β relationship is the same along each path. This leads to γ values that are somewhat larger for the NTS-ALQ path. To reduce the discrepancy between the ALQ and TUC inferred Ψ_∞ , the difference between the γ values would have to be larger still. For example, if $\gamma(\omega)$ were about 10^{-4} km^{-1} larger at periods of interest for the NTS-ALQ path and the same amount smaller for the NTS-TUC path, the inferred average TUC Ψ_∞ /ALQ Ψ_∞ ratio would drop from 1.56 to 1.32. Changes in γ of this amount are plausible, but at this time cannot be justified by any independent information. The amplitude discrepancy we see may be viewed as a good indication that our γ estimate is too low for NTS-ALQ and/or too high for NTS-TUC, but this question cannot really be resolved without more research.

In Sections V and VI we showed synthetic seismograms for a variety of source configurations. The match of synthetic and observed seismograms achieved for ALQ was excellent. The match to the TUC observations was more sensitive to details of the source, but in most cases was also quite good. However, our synthetic records never match the long period (≈ 10 to 12 seconds) cycles just ahead of the Airy phase. Comparison

of theoretical and observed spectra indicate that this mismatch might be due to there being too little long period energy in the synthetic spectra. To test this hypothesis, we constructed a $\gamma(\omega)$ which brings the theoretical and observed amplitude spectra into better agreement. The $\gamma(\omega)$ and the resulting seismogram for the Yucca Flat explosion source are shown in Figure 25.

The new seismogram in Figure 25 gives an excellent fit to the observed record. If we applied the same $\gamma(\omega)$ to the best composite source record of Figure 21 (Case G), the fit would be even better. However, the peculiar $\gamma(\omega)$, which is peaked near 9 seconds, implies extreme depth variations in Q compared to the models in Figure 8 and may even imply negative Q at some depths.

Since the fit to the observations is enhanced with the special $\gamma(\omega)$ in Figure 25, we must either suppose that this $\gamma(\omega)$ is accounting for both anelastic and scattering effects, possibly with a frequency-dependent Q, or that this $\gamma(\omega)$ is compensating for errors in our specification of the source and path amplification. However, the kinds of models used in this study are unlikely to be able to account for spectral shaping like that represented by the special $\gamma(\omega)$. Further, the synthetic and observed spectra are in good agreement at ALQ, providing evidence that the error is not in the source specification. We are, therefore, inclined to attribute the disagreement of the long period portion of the observed and synthetic records at TUC to the inability of our rather simple plane-layered models to perfectly represent the real earth.

In summary, the fit to the TUC seismograms is not quite as good as for the ALQ records. This is true both for the dispersion and for the amplitude spectrum. We believe the result is to cause an overestimate of the source amplitude required to match the TUC data, though this cannot be conclusively demonstrated. The more dispersed seismograms at

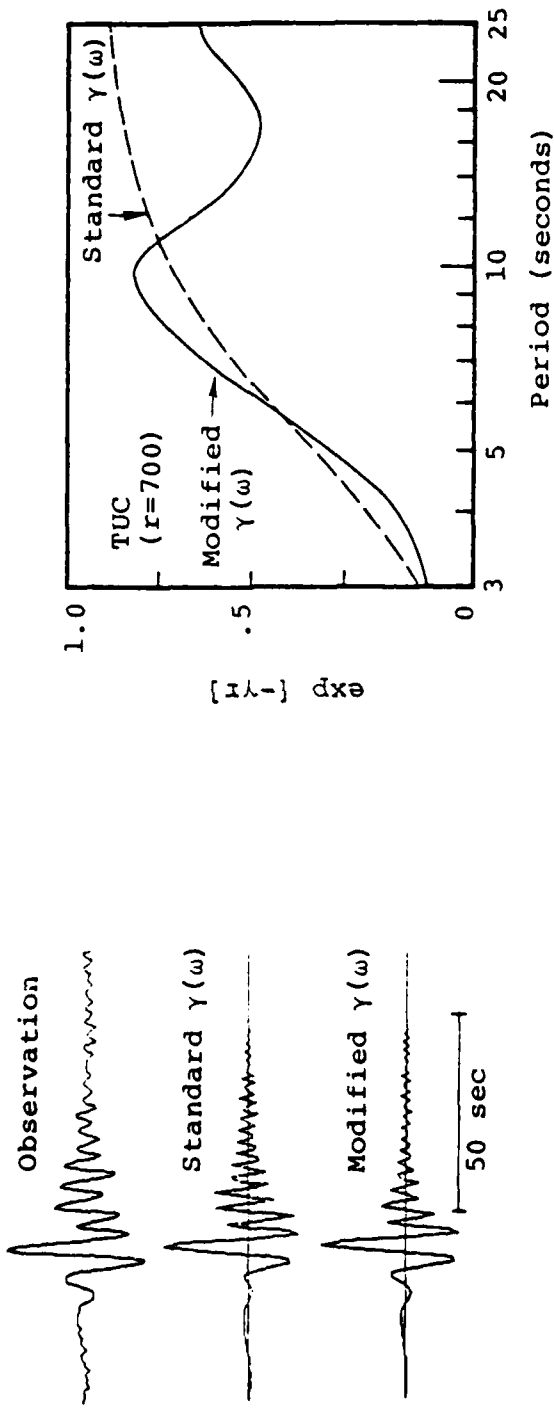


Figure 25. The observation of the Yucca Flat event TAN at TUC is compared to synthetic seismograms computed with two attenuation models. The source is a reduced displacement potential and the "standard $\gamma(\omega)$ " seismogram is that shown in Figure 5.

ALQ are fit very well and it is tempting to prefer the Ψ_∞ inferred from these data. On the other hand, the NTS-TUC path is in one tectonic province while the known lateral variations along the NTS-ALQ path are much larger. These lateral variations would probably cause us to underestimate the source amplitude required to match the ALQ data. Finally, the Q models used for the two paths could easily include errors that would cause the amplitude estimates to change by 20 to 30 percent. Changes much larger than that seem unlikely.

Considering all these factors, the difference in the source estimates from the two stations is not surprising. The true value is probably somewhere between the two, though we give somewhat more credence to the ALQ estimates. As is so often the case, a better definition of the answer can probably only be obtained by going through the same process for more stations so random uncertainties can be reduced by averaging.

VIII. CONCLUSIONS

Our purpose in this work was to explore in as much detail as possible the usefulness of synthetic seismogram techniques for studying underground nuclear explosions and, particularly, for determining their yield. To do so, we have used observations at two particular stations to determine the Ψ_∞ for NTS explosions. The relationship between Ψ_∞ and explosion yield is dependent on the source material properties and is a separate issue not discussed here.

The capability to determine the Ψ_∞ from comparison of synthetic and observed seismograms was conclusively demonstrated. There are uncertainties and unresolved issues, but we have attempted to carefully bound the range of uncertainty and to pose the questions that remain unanswered.

The key features of this work may be summarized as follows:

- Surface wave observations of explosions can be used to infer models for the earth structure along the travel path. These models then predict synthetic seismograms that closely resemble the observed records.
- The amplitude of the source can be inferred by comparing synthetic and observed records. For Yucca Flat and Pahute Mesa events, the inferred source amplitude is in general agreement with values obtained by other methods.
- The effect of spallation was carefully explored. The spall closure impulse is too small to have much influence. More likely to be important is the loss of energy from the upgoing waves that is associated with spallation.
- The extent to which the upgoing waves are attenuated by spallation or scattered is poorly understood. For the wavelengths of interest, it may not even occur to a significant extent. More theoretical work is required to resolve the questions.

Particularly useful would be the study of Rayleigh waves from two-dimensional finite difference calculations in which spall is allowed.

- Tectonic strain release will affect the source estimates, but it can be corrected if sufficient azimuthal coverage is available.
- The important PILEDRIVER event is, unfortunately, the most puzzling of those studied. The tectonic release and spall related phenomena dominate the source determination. The agreement of synthetic and observed waveforms is significantly worse for this event, suggesting that something might be unaccounted for in the vicinity of the source.
- The source level for the Yucca Flat events is best determined. A substantial proportion of the deviation from the mean Ψ_∞ for individual events is probably associated with real differences in the source coupling. It is important to know how large these differences can be for superficially identical events (individual Ψ_∞ values are given by Bache, 1978).
- The source level for Pahute Mesa events is determined with less confidence than for Yucca Flat because of larger uncertainties associated with tectonic release and spallation phenomena. Also, relatively few Pahute Mesa events were examined.
- Finally, we point out that our data for this study was taken from WWSSN film clips. This is far from ideal for many reasons, especially in the narrow yield range to which we were restricted. Digital data from well-maintained stations would be much better.

Applying the techniques of this report to foreign explosions, we would obtain a yield estimate that is independent of the estimate from empirical M_S -yield curves. Of course, the two estimates would be the same if the empirical data were not biased by some systematic factor that was correctly accounted for by our more detailed modeling procedure. The uncertainties in yield estimates from the matching of synthetic and observed records may be summarized as follows:

1. Different estimates would be obtained from different stations. After correcting for radiation pattern effects, taking Love waves into account, these would be averaged and a statistical estimate of the uncertainty would result.
2. Neither the velocity nor Q models will ever be determined with ideal accuracy. We can estimate the errors associated with uncertainties in these models and the models themselves should improve with time if the effort is made.
3. The most important uncertainties are associated with the source itself. First, there is the relationship between the source amplitude and the explosion yield. However, the most that can ever be determined with seismic methods is the source amplitude. Second, there are the uncertainties associated with the selection of the appropriate model for the spallation process and, particularly, the loss of energy from the upgoing waves. More research will help resolve these questions. Also, we point out that there is no reason to suppose foreign and U.S. explosions would be much different as far as this aspect of the physics is concerned.

If we select a particular model for this process (for example, assuming that 25 percent of the upgoing waves are suppressed) and interpret U.S. and foreign events with this assumption, our source amplitude estimates will be consistent.

ACKNOWLEDGMENT

We gratefully acknowledge the assistance of several of our colleagues at Systems, Science and Software. The Airy phase amplitude measurements were made by Dr. John Savino and Mr. David Lambert. Discussions with Professor David Harkrider and Dr. Henry Swanger helped clarify a number of difficult issues. The manuscript was typed by Ms. Tracy Reiter and Ms. Carolyn Hunt prepared the figures.

REFERENCES

Aki, K. and Y. Tsai (1972), "The Mechanics of Love Wave Excitation by Explosive Sources," J. Geophys. Res., 77, pp. 1452-1475.

Aki, K., M. Bouchon and P. Reasenberg (1974), "Seismic Source Function for an Underground Nuclear Explosion," Bull. Seism. Soc. Am., 64, pp. 131-148.

Archambeau, C. B. (1972), "The Theory of Stress Wave Radiation from Explosions in Prestressed Media," Geophys. J., 29, pp. 329-366.

Bache, T. C., J. T. Cherry, N. Rimer, J. M. Savino, T. R. Blake, T. G. Barker and D. G. Lambert (1975), "An Explanation of the Relative Amplitudes Generated by Explosions in Different Test Areas at NTS," Systems, Science and Software Final Report to the Defense Nuclear Agency, DNA 3958F, October 1975.

Bache, T. C., P. L. Goupillaud and B. F. Mason (1977), "Seismic Studies for Improved Yield Determination," Systems, Science and Software Quarterly Technical Report submitted to ARPA/VSC, July.

Bache, T. C. (1978), "A Detailed Listing of the Data and Results for the Unclassified Report: Source Amplitudes of NTS Explosions Inferred from Rayleigh Waves at Albuquerque and Tucson," Systems, Science and Software Topical Report.

Bache, T. C., W. L. Rodi and D. G. Harkrider (1978), "Crustal Structures Inferred from Rayleigh Wave Signatures of NTS Explosions," Bull. Seism. Soc. Am., 68 (in press).

Cherry, J. T., N. Rimer and W. O. Wray (1975), "Seismic Coupling from a Nuclear Explosion: The Dependence of the Reduced Displacement Potential on the Nonlinear Behavior of the Near Source Rock Environment," Systems, Science and Software Technical Report, AFTAC/VSC, SSS-R-76-2742, September.

Chilton, F., Eisler, J. D. and H. G. Heubach (1966), "Dynamics of Spalling of the Earth's Surface Caused by Underground Explosions," J. Geophys. Res., 71, pp. 5911-5919.

Eisler, J. D. and F. Chilton (1964), "Spalling of the Earth's Surface by Underground Nuclear Explosions," J. Geophys. Res., 69, pp. 5285-5293.

Eisler, J. D., F. Chilton, and F. M. Sauer (1966), "Multiple Subsurface Spalling by Underground Nuclear Explosions," J. Geophys. Res., 71, pp. 3923-3927.

Harkrider, D. G. (1964), "Surface Waves in Multilayered Media I. Rayleigh and Love Waves from Buried Sources in a Multilayered Elastic Half-Space," BSSA, 54, pp. 627-679.

Harkrider, D. G. (1970), "Surface Waves in Multilayered Media II. Higher Mode Spectra and Spectral Ratios from Point Sources in Plane-Layered Earth Models," Bull. Seism. Soc. Am., 60, pp. 1937-1987.

Harkrider, D. G., C. A. Newton and E. A. Flinn (1974), "Theoretical Effect of Yield and Burst Height of Atmospheric Explosions on Rayleigh Wave Amplitudes," Geophys. J., 36, pp. 191-225.

Haskell, N. A. (1967), "Analytic Approximation for the Elastic Radiation from a Contained Underground Explosion," J. Geophys. Res., 72, pp. 2583-2587.

Lambert, D. G., E. A. Flinn and C. B. Archambeau (1972), "A Comparative Study of the Elastic Wave Radiation from Earthquakes and Underground Explosions," Geophys. J., 29, pp. 403-432.

Minster, J. B. and A. M. Suteau (1977), "Far-Field Waveforms from an Arbitrarily Expanding Transparent Spherical Cavity in a Prestressed Medium," Geophys. J., 50, pp. 215-233.

Mitchell, B. J. (1975), "Regional Rayleigh Wave Attenuation in North America," J. Geophys. Res., 80, pp. 4904-4916.

Murphy, J. R. (1974), "Discussion of Seismic Source Function for an Underground Nuclear Explosion by Keiiti Aki, Michel Bouchon and Paul Reasenberg," Bull. Seism. Soc. Am., 64, pp. 1595-1597.

Orphal, D. L. (1970), "The Cavity Formed by a Contained Underground Nuclear Detonation," NVO-1163-TM-15, AEC.

Perret, W. R. (1968), "Free Field Ground Motions in Granite," Operation Flintlock, Shot PILEDRIVER, DASA POR-4001.

Sobel, P. A. (1978), "The Effects of Spall on m_b and M_s ," unpublished Teledyne Geotech Report.

Springer, D. L. and R. L. Kinnaman (1971), "Seismic Source Summary for U. S. Underground Nuclear Explosions, 1961-1970," Bull. Seism. Soc. Amer., 61, pp. 1073-1098.

Tsai, Y. B. and K. Aki (1971), "Amplitude Spectra of Surface Waves from Small Earthquakes and Underground Nuclear Explosions," J. Geophys. Res., 76, pp. 3940-3952.

Toksöz, M. N., K. C. Thomson and T. J. Ahrens (1971), "Generation of Seismic Waves by Explosions in Prestressed Media," Bull. Seism. Soc. Am., 61, pp. 1589-1623.

Toksöz, M. N. and H. H. Kehrer (1972), "Tectonic Strain Release by Underground Nuclear Explosions and its Effects on Seismic Discrimination," Geophys. J., 31, pp. 141-161.

Toman, J., C. Sisemore and R. Terhune (1973), "The RIO BLANCO Experiment: Subsurface and Surface Effects and Measurements," Lawrence Livermore Laboratory Report, UCRL-51504.

Viecelli, J. A. (1973), "Spallation and the Generation of Surface Waves by an Underground Explosion," J. Geophys. Res., 78, pp. 2475-2487.

Von Seggern, D. H., P. A. Sobel and D. W. Rivers (1975), "Experiments in Refining M_s Estimates for Seismic Events," Teledyne Geotech Report SDAC-TR-75-17, November 1975.

Werth, G. C. and R. F. Herbst (1963), "Comparison of Amplitudes of Seismic Waves from Nuclear Explosions in Four Mediums," J. Geophys. Res., 68, pp. 1463-1475.